NASA MEMO 1-6-59L

NASA

MEMORANDUM

INVESTIGATION OF SPHERICAL-WAVE-INITIATED FLOW FIELDS AROUND BODIES

By Donald R. McFarland

Langley Research Center
Langley Field, Va.

NATIONAL AERONAUTICS AND SPACE ADMINISTRATION
WASHINGTON
February 1959

NATIONAL AERONAUTICS AND SPACE ADMINISTRATION

MEMORANDUM 1-6-59L

INVESTIGATION OF SPHERICAL-WAVE-INITIATED FLOW FIELDS AROUND BODIES

By Donald R. McFarland

SUMMARY

Measurements of the velocity flow fields and vortex movements have been made about various simple blunt models undergoing spherical blast waves with a positive overpressure of 4 pounds per square inch. A bullet-optical method was used to determine flow velocities and is applied to velocity fields in which the gradients are largely normal to the free-stream direction.

The velocity flow fields are shown at various flow times following passage of the blast front for different models. Vortex movements with time are compared for square-bar models of various aspect ratios. Corner sharpness had no discernible effect on the overall disturbed velocity fields or vortex movements for the square-bar models used.

INTRODUCTION

In order to design blast-resistant bodies and structures, it is necessary first to understand the transient loading which may be imposed on the body as a result of the blast wave and blast-induced flow. For blast waves of low overpressure, the problem is usually separated into two phases. The first is the diffraction phase consisting of loadings due to the shock-front interaction with the body, and the second is the drag phase where the loading results from the fluid motion about the body. The diffraction phase involves the larger forces on the body but is of relatively short duration (a few body diameters of the blast front travel) and for a given overpressure is independent of the energy yield of the charge. The drag phase involves forces which are limited to the order of the dynamic pressure of the fluid following the blast front, but impulsewise they may be greater than the diffraction phase if the duration of exposure is relatively longer. Since the rate of overpressure decay with time is set by the yield of the charge, the relative magnitude of the diffraction and drag loadings at a given overpressure is a function of the initial energy yield of the charge.

With the onset of blast-induced flow over a body, vortices are produced in cases where there is a sharp turning in the flow about the body. The effects of these vortices and their affiliated low-pressure fields are important to the loading of the body as these vortices move with time. Considerable experimental work has been done with the use of shock tubes to study such flow fields about bodies. (See refs. 1 to 6.) A more general bibliography for the blast-loading problem is found in reference 7. In most of these shock-tube studies two-dimensional bodies were mounted in the shock tube and interferometric techniques were used to determine density gradients at various flow times about the bodies. There has been some effort to use fast-response piezoelectric gages on a model such as the work presented in reference 8.

The blast-wave table provides a true spherical blast-wave flow; that is, a "peaked" blast with three-dimensional flow as opposed to the so-called "flat-topped" wave of a shock tube where the flow behind the shock front is ideally one dimensional with constant pressure and velocity. However, close simulation of the blast flow can be made with a shock tube for cases where the time decay of pressure and velocity is small during the flow times of interest. The flat-topped wave of the shock tube should be particularly useful for the diffraction phase of the flow where the flow times are short and the flow has not yet been appreciably altered by the shock-tube wall effects. The blast flow on a blast-wave table, on the other hand, may be free of wall effects for long flow times relative to the positive duration time. Reference 9 shows a method used in a shock tube to produce one-dimensional peaked blast waves by means of shaped charges of primacord.

The purpose of this study was to find, by a unique optical method, the flow velocity distribution and vortex travel about simple models for actual spherical blast-wave conditions. Although this method does not directly give the forces on the body, such a method, in conjunction with density measurements, would yield force data for the case of two-dimensional flows. This unique method involved the use of a bullet bow-wave distortion due to local flow conditions. This bullet-optical method was developed and described in reference 10 for adaption to boundary-layer studies. The method is applied here to the blast-flow phenomena of a small-scale spherical blast wave conducted on the blast-wave table of the Langley gas dynamics laboratory.

SYMBOLS

a	velocity of sound
b	constant for a given blast-wave-peak overpressure, $p_2 - p_0$

F	bow-wave parameter, $\frac{2}{\gamma - 1}\left(\frac{\sin i}{M_n}\right)^2$
i	bow-wave incidence angle
k	model height
l	fluid particle movement in blast direction
M	Mach number
p	absolute pressure
r	radial distance from bullet axis
t	time from blast front encounter with a specified point $t = 0$ at $l = 0$
t'	time during which there has been blast-induced flow at a fixed radius from blast origin
t_d	positive-overpressure time duration of blast wave at a fixed radius from blast origin
T	absolute temperature
u	velocity
V	shock-wave velocity (blast front)
x	horizontal distance in flow direction from leading edge of model at $y/k = 1$
y	distance normal to flow
γ	ratio of specific heats

Subscripts:

0	initial flow ($t < 0$)
2	blast flow immediately behind shock wave
B	bullet
n	normal to bow wave

W bullet bow wave

β free-stream blast flow

BULLET THEORY

When the bullet technique is applied to the measurement of flow variations, use is made of the fact that a weak bullet bow wave approaches the character of a Mach wave; hence, when the wave slope and the bullet velocity are known, it is possible to determine the local flow velocity. The development of this technique is discussed in detail in reference 10. The theory will be reviewed only briefly here in its application to the blast-wave flow.

A bullet is fired upstream through a blast wave, as shown in the following sketch:

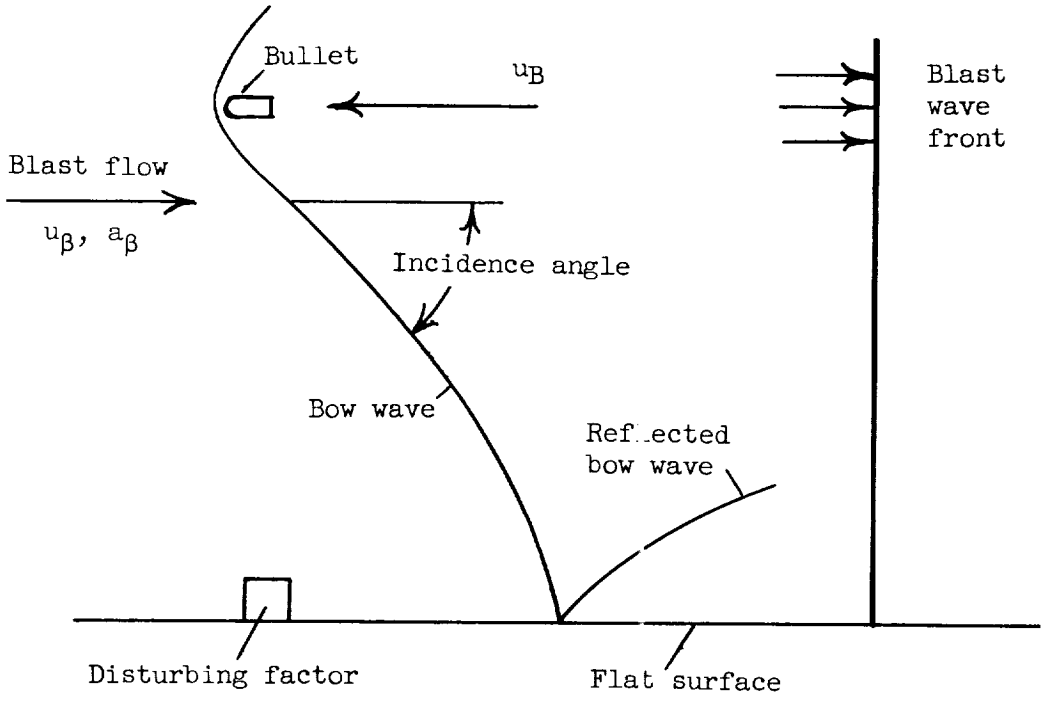

The Mach number of the bullet, with respect to the fluid in the blast flow, is then

$$M_B = \frac{u_\beta + u_B}{a_\beta} \tag{1}$$

If the streamwise variation of the fluid flow is assumed to be small in comparison with the variation normal to the fluid flow, the Mach number normal to the bullet wave is

$$M_n = M_B \sin i \geqq 1.0 \tag{2}$$

provided that the bullet wave has been generated within the blast-flow region. The variations of the fluid velocity, speed of sound, and pressure behind the blast wave, which are developed in the appendix, are:

$$\frac{u_\beta}{u_2} = \frac{1 - \frac{t'}{t_d}}{e^{\frac{1}{2}\frac{t'}{t_d}}} \tag{3}$$

and

$$\frac{a_\beta}{a_2} = \left(\frac{p_\beta}{p_2}\right)^{1/7} = \left(\frac{1 - \frac{t'}{t_d}}{e^{\frac{3}{4}\frac{t'}{t_d}}}\right)^{1/7} \tag{4}$$

By assuming no heat transfer from the wall, as in reference 10, and adopting blast-wave flow conditions, the equation for the locally disturbed velocity expressed nondimensionally in terms of local undisturbed blast flow can be written as:

$$\frac{u}{u_\beta} = \frac{-2F\frac{u_B}{u_\beta} + \sqrt{\left(2F\frac{u_B}{u_\beta}\right)^2 - 4(F+1)\left[F\left(\frac{u_B}{u_\beta}\right)^2 - 1 - \frac{2}{(\gamma - 1)M_\beta{}^2}\right]}}{2(F+1)} \tag{5}$$

where

$$F = \frac{2}{\gamma - 1}\left(\frac{\sin i}{M_n}\right)^2$$

Since, at a fixed point, the free-stream velocity of the blast flow is changing with time because of the blast-wave movement, it is desirable to express the local fluid velocity in terms of a constant reference

velocity. The constant used is the velocity immediately behind the blast front at the time the front reaches the model; that is, u_2 at $t = 0$. Therefore, the nondimensional local velocity is given by

$$\frac{u}{u_2} = \frac{u}{u_\beta}\frac{u_\beta}{u_2} \tag{6}$$

By using these relations, the local velocities about bodies in a blast may be found from measurements of the bullet velocity and bow-wave shape.

Because the bow wave generated by the bullet is propagated at a lower angle of incidence upon entering the blast flow, equation (2) is not rigorous for that portion of the bow wave which was generated ahead of the blast wave and propagated into the blast flow. This limitation can be overcome if it is assumed that the strength of the bullet wave M_n is not changed upon passing through the blast front. Equation (2) is then solved for an apparent bullet velocity which is appropriate to this portion of the bullet bow wave. For this data, however, it has been found that errors in velocity of less than 10 percent result from applying equation (2) directly to the portion of the wave rising from the actual bullet velocity and equation (2) was therefore used.

Since there are gradients of u and a in the direction of the blast flow for the spherical blast wave, it should be noted that the wave incidence angle is not strictly the ratio of normal Mach number to the Mach number of the wave relative to the stream. (See the discussion of this case in ref. 10.) Although these streamwise gradients of u and a are perceptible in that part of the flow field encompassed by the bullet wave, it was felt that, except for large local gradients such as those near vortices, use of the method would not be seriously restricted. The most serious limitation is the error that occurs when the local fluid flow direction varies greatly from that of the free stream.

APPARATUS AND PROCEDURE

The apparatus used for these experiments was the blast-wave table at the Langley gas dynamics laboratory. A schematic diagram of the instrumentation and layout of the blast-wave table and rifle arrangement is shown in figure 1. A 12-foot-square table was fabricated from two-inch-steel boiler plate which was machined smooth and flat on the upper surface and was extended along the blast line by the addition of 1/2-inch-thick end-plate extensions. The table was supported rigidly by a system of large I-beams that were imbedded in concrete so that the

under surface of the table was accessible for mounting the pressure instrumentation and the running of electrical leads.

The blast waves were created by $13\frac{1}{2}$-gram spherical cast, bare, 50/50 pentolite charges. The charges were detonated by instantaneous electric blasting caps inserted and bottomed in a detonator well in the charge; the well was 5/16 inch in diameter and 6/10 inch deep. The detonator was fired by the discharge of a capacitor which was charged to 2,000 volts and discharged through a thyratron circuit. The combination of charge and detonator resulted in an equivalent total-energy release of 14.45 grams of pentolite, the variation from the average equivalent weight being approximately ±0.6 grams.

The charge with the detonator was suspended from a support arm at a height of 2 feet above the table by putting the charge in a mesh net which could be hung on an adjustable metal hook located in the support arm. The axis of the detonator cap was set perpendicular to the blast line and parallel to the table top. The support arm was a crescent-shaped plate of 1/2-inch steel located in a plane perpendicular to the blast line and far enough from the center of burst so that no blast-wave reflection from the support arm would reach the test area during the time of interest.

From each test run, a schlieren photograph and time data were taken to obtain blast-front speed, blast-front position or model flow time, bullet speed, and bullet-bow-wave profile. The schlieren optical system consisted of a high-voltage spark source, two 6-inch-diameter parabolic mirrors of 20- and 36-inch focal length for the source and knife-edge mirrors, respectively, a vertical mirror knife edge, and an 8- by 10-inch film holder. All the optical components were shielded from the blast light and room lights during a test.

The blast-wave strength was determined for each run by the wave velocity as indicated by pressure pickups which were a known distance apart and were mounted flush with the surface of the wave table along the blast line. By detonating the charge at a height of 2 feet above the table, a peak overpressure of 4 pounds per square inch could be attained at the model at a ground distance of 7.61 feet from the charge. Also at this distance, it should be noted that the blast front is well into the Mach reflection region and the triple point has risen to a height of 6.2 inches, which is above the view of the schlieren system. The pressure pickups used were flush-mounted, capacitor types which used frequency-modulated carriers with diaphragms whose natural frequency was approximately 10,000 cycles per second. The output of the pressure pickups was recorded on a four-channel oscilloscope and drum camera and the data were used to find the pressure time history of the blast wave. The positive time duration was established from these

pressure records for the undisturbed flow case (no model) and was found to be 900 microseconds for the model at a distance of 7.61 feet. A measurement of the time lapse was made from the blast front arrival at the last pressure pickup before the model to the time the schlieren photograph was taken to provide a means for obtaining the model flow times, particularly for the runs where the blast front had passed out of the schlieren field.

The velocity distributions in the blast flow were determined from the slope of the bow wave from 22-caliber long-rifle hollow-point bullets which were selected because they best fitted the velocity requirements from commercial stock. The bullets were fired upstream along the blast line about 4 inches above the table and were positioned in time with the blast by means of a series of electronic pickup stations and delay units. A typical time history plot is shown in figure 2. A time-interval counter which would read back a time equal to the time counted was incorporated to compensate for the variable bullet velocity from run to run. This unique configuration of timers functions as follows: The base delay is preset so as to be always less than the arrival time of the bullet at the second station. The bullet-discrepancy-time counter then first counts this time difference and then counts back the identical time before actuating the charge delay unit. Thus, the firing of the charge is done earlier or later than the average time by an interval of time double the change of bullet discrepancy time from the average time. Since the bullet has traversed only half the distance to the model at this second station, it likewise arrives at its destination off the average time by an amount of time double this change in bullet discrepancy. A charge-time delay unit is used to predetermine the position of the blast wave with respect to the bullet with a total tolerance of ±10 microseconds. The spark-delay unit is likewise preset to photograph the bullet wave at the time the bullet is in position with respect to the model. Light cut-off photoelectric cell stations were used for the bullet pickup and velocity-measuring stations.

The models tested are listed in table I for quick reference. Model 1 was a ground-finish steel bar 6 inches long and ground to 1/4 inch square with a corner radius not more than 0.002 inch. Models 2 and 3 were a 6-inch long and a 2-inch long piece of regular one-quarter-inch square steel bar stock which were found to have corner radii from 0.015 to 0.018 inch. The fourth model was a one-half-round brass bar 6 inches long with a radius of 1/4 inch.

RESULTS AND DISCUSSION

Schlieren Photographs

Schlieren photographs were taken with the bullet bow wave in various positions with respect to the model at different increments of model flow time. A sample photograph is shown in figure 3 to acquaint the reader with the complete schlieren data picture. The blast front passes from left to right. Since the triple point is well above the field of view the blast front appears to be fairly straight except for the distortion near the table surface produced by the model. Reflections of the blast front from the model are seen propagating out from the model. Vortices from the leading and trailing edges of the model are clearly seen at the model; each was dark on one side and light on the other because of the vertical schlieren knife edge used.

Although the bullet has passed out of the picture to the left, its wake still shows at the top of the picture and its bow and tail waves extend to the table surface and are reflected. From enlargements of photographs like this, the bullet bow-wave angles and position were measured for the velocity profile data and vortex positions determined.

A series of schlieren photographs with model 1 is shown in figure 4 in a sequence of increasing flow times after the blast front arrived at the model to illustrate vortex movement. The bullet bow wave is shown at various positions near the model to illustrate wave profiles that were obtained. A series of pictures is also shown for each of the other models tested in figures 5 to 7.

There are various minor disturbances that appear in the schlieren field, most of which are not in the immediate flow field of the model. The first disturbance known to enter the model blast flow field is a weak reflection of the blast front from the calibrating pin support at the edge of the table that arrives at the model at about $t = 760$ microseconds and can be found in the last pictures of figures 4, 5, and 7. An interesting effect showing dust-particle movement appeared when an unnoticed accumulation of dust on the table was caught in flight around the model by the schlieren photographs. This effect can be seen in figure 5 at times $t = 268$ microseconds to $t = 643$ microseconds.

One result of the three-dimensionality of the blast can be seen in the photographs showing the blast front (the first pictures of figs. 4 to 7). For the low-aspect-ratio model (fig. 6) the blast front passes by the ends of the model and obscures the portion of the blast front near the table surface that has been distorted by the model, whereas for the long model this distortion is partially seen as the blast front passes the end of the model at a slightly later time. The vortices for

the short model (fig. 6) seem to dissipate more rapidly with time than those for the long model with the same corner radius (fig. 5). For the half-round model, no vortex formation or movement is apparent in the pictures (see fig. 7); however, a separated flow region is seen to develop at the model at some interval of time after the shock front has passed.

Computed Velocity Fields

For each run the bullet bow-wave angle was determined from an enlargement of the schlieren photograph and was plotted as a function of radial distance from the bullet path; a sample plot is shown in figure 8. To this plot was added an estimated undisturbed bullet-wave profile based on data taken in the blast flow without the model disturbance. By using the angles from the curves of this plot, the nondimensional velocity was calculated from equations (5) and (6) and was plotted to show the variation along the bullet wave. A sample plot is shown in figure 9.

In order to show a more representative picture of the flow field about the model, a number of runs were compiled into composite plots. These composite plots are shown in figures 10, 11, and 12 for models 1, 2, and 4, respectively, and approximate contours of equal velocity are drawn on these plots. Since the blast flow field varies with time and space, and since it was very difficult to repeat tests at exactly the same model flow times, the composites include photographs taken within a given range of flow times. This variation of flow time was taken into consideration during the drawing of the velocity contour for an average flow time. Limits of the free-stream flow variations due to the different blast flow times used for each composite are shown in the free-stream portion of the velocity contour at the top of each figure. The large circles show the region of a vortex whereas the crossmarks (+) signify the positions of the vortex center for each test represented in the figure.

The blast-wave-front reflection from the model that can be seen moving out into the blast flow in figure 3 was found to be traveling out from the model just slightly faster than the local speed of sound and it is felt these reflections have little measurable influence on the composite plots.

It is seen from these plots that the flow field appreciably affected by the model is within about four model heights and seems to become slightly smaller with time. Immediately downstream of the model the velocities are affected by a down flow as the stream flows over the model and appear to have nearly recovered to the stream velocity by 4 to 5 model heights downstream. Of course, end effects about the model are present

but cannot be resolved in these two-dimensional pictures. The velocities in the affected regions are in all cases less than the free-stream velocities except over the leading edge and in the immediate vicinity of a vortex and diminish with time as does the free stream.

It appears that this bullet-optical method works rather well where the gradients of the velocity field are largely normal to the free-stream flow direction, since the undisturbed blast velocities found by this method are very close to those of the blast theory. However, for large gradients in the stream direction, such as those due to the large radial velocity gradients in a vortex, the bullet-wave theory breaks down. This can clearly be seen in some of the photographs of figures 4, 5, and 6, where the bullet wave has interacted with a vortex. The rotation of the vortices in a clockwise direction is shown by the more rapid advancing portion of the bullet wave below the center of vortices. With the accuracy obtained there do not seem to be any outstanding differences between the composite velocity plots for the sharp-edged square model and the regular square-bar model. An increase in flow velocity is seen above the leading edge in all three configurations shown. Because of the interaction of the bullet bow wave with the model, no data are shown upstream of the model.

The area of the affected flow field over the half-round model does not appear to be much different from that over the square-bar models; however, the lack of vortices provides a much cleaner flow for use with this bullet technique. As seen in the photographs, flow separation appeared only at the later flow times. The presence of the reversed flow field downstream of the separation point is indicated on figure 12(b); however, because of the limited amount of data for this configuration, the extent of the reversed flow region is not clearly established.

Vortex Positions

The position of the leading-edge vortex center has been plotted as a function of time. Figure 13 compares the horizontal component (free-stream direction) of the leading-edge vortex movements of models 1, 2, and 3 in terms of the positive time duration of the blast. There seems to be no significant difference in movement of the vortex center because of the differences of leading-edge radii or of the lengths of the models used. The vortex produced by the sharp-edged model (model 1) seemed to be more clearly defined than that for model 2. The vortex produced by the short model (model 2) dissipated more rapidly with time and was not distinguishable at the later times. It can be noted that the leading-edge vortex center never reaches the trailing edge and it appears to have stopped its downstream travel before the positive time duration has passed. However, the vortex has dissipated by this time (approximately $0.8t/t_d$) so as to make its center hard to distinguish. The

vertical component (normal to free-stream blast flow) of leading-edge vortex movement is shown in figure 14. The horizontal and vertical components of the trailing-edge vortex movements with time are plotted in figures 15 and 16, respectively. The trailing-edge vortex reverses in direction of movement at about one-half of the positive time duration. This reversal, of course, would indicate a strong backflow under the vortex. This backflow would account for the large increase in propagation of the bullet wave beneath the vortex.

The schlieren photographs indicate that the leading-edge vortex dissipates faster than the trailing-edge vortex. After about 700 microseconds the center of the leading-edge vortex is very difficult to distinguish, whereas the trailing-edge vortex which is shielded from the flow by the model is still very well defined. A comparison of the movement of the vortex centers in the free-stream direction is made relative to the free-stream particle movement and is shown in figure 17. The blast flow (free-stream) fluid movement is determined by the method given in the appendix and the results of this computation are shown in figure 18. It can be seen from figure 17 that the vortices are traveling much slower than the free-stream fluid. Also, the vortices are slowing down with respect to the free-stream particle movements, except for the initial trailing-edge vortex movement.

CONCLUSIONS

A bullet-optical technique was used to obtain measurements of the velocity flow fields and vortex movements about various blunt-shaped bodies undergoing a spherical blast wave with a peak positive overpressure of 4 pounds per square inch.

1. It appears that the blast flow is not greatly affected by the model outside a radius of 4 to 5 model heights and that the flow velocities outside this region determined by this method are close to that provided by blast flow theory.

2. Except for a region above the leading edge of the model, the velocities in the disturbed region remain below that of free-stream velocity and both diminish with time after blast front passage.

3. It was found that the vortices formed at the leading and trailing edge of the model at blast encounter traveled at far less than free-stream velocities and slowed down with respect to the free-stream flow. The leading-edge vortex never reached the trailing edge and the trailing-edge vortex actually reversed its movements as though in a backflow behind the model. The movements of the vortices with time appeared to

be unaffected by the corner sharpness or length of the three square-bar models used.

4. In all cases, the leading-edge vortex dissipated more rapidly in the stream than the trailing-edge vortex, which was protected from the fluid stream by the model. The vortices, however, produced by the sharp-edged model seemed to be a little more clearly defined and those produced by the short model dissipated more rapidly with time.

5. Although no vortices are clearly established for the half-round-model flow, a flow separation is seen to occur at a relatively late flow time.

Langley Research Center,
National Aeronautics and Space Administration,
Langley Field, Va., September 22, 1958.

APPENDIX

COMPUTATION OF BLAST FLUID FLOW

For a spherical blast wave the variation of overpressure at any point is a function of time and up to a value of t'/t_d of 2 may be expressed as:

$$\frac{p - p_0}{p_2 - p_0} = \frac{1 - \frac{t'}{t_d}}{e^{b\frac{t'}{t_d}}} \tag{A1}$$

where b is a constant for a given blast-wave-peak overpressure $p_2 - p_0$. (A value of $b = 3/4$ is found to be representative of the case when $p_2 - p_0 = 4$ pounds per square inch.) This expression has been suggested in a number of places in the literature (for example, see ref. 11) and was found to fit closely the pressure-time curves available. The value of b may be found by evaluating equation (A1) at $\frac{t'}{t_d} = 2$ by using values of the peak negative overpressure from reference 12.

If it is assumed that, in the region behind the spherical shock wave $\left(0 < \frac{t'}{t_d} < 1.0\right)$, the fluid entropy is constant $\left($a reasonable assumption for the weaker shock cases, $\frac{p_2}{p_0} < 2.0\right)$, then the relation between fluid velocity and overpressure is found from Riemann's isentropic unsteady flow relations, which for air (when $\gamma = 1.40$) yields

$$\frac{u}{u_2} = 1 + \frac{5}{M_2}\left[\left(\frac{p}{p_2}\right)^{1/7} - 1\right] \tag{A2}$$

The value of M_2 is found as a function of $\frac{p_2}{p_0}$ from the Rankine-Hugoniot shock relations applied to this case.

It can be shown by numerical substitution that equations (A1) and (A2) are very closely satisfied over a range of blast-wave overpressures, $0 < p_2 - p_0 < 20$ pounds per square inch, by the following relation:

$$\frac{u}{u_2} = \frac{1 - \frac{t'}{t_d}}{e^{\frac{1}{2}\frac{t'}{t_d}}} \tag{A3}$$

This equation represents an approximation of the variation of fluid velocity at any fixed reference point as a function of time, being measured from the time of shock passage at this same point. In order more readily to find the position with time of a particular particle of fluid, the time is now referenced to that of shock passage at a specified fixed point and certain simplifications are made. See the following sketch.

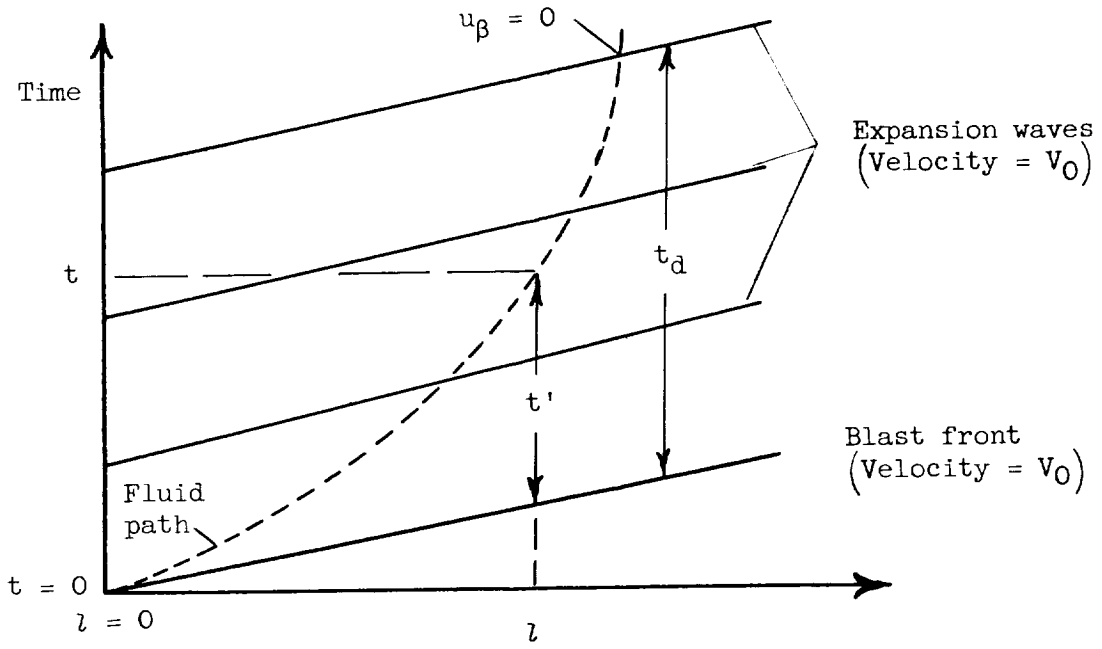

Fluid particle movement along a radial line through blast origin

It is assumed that over a short increment of the total blast travel, the blast front travel may be assumed to be at a constant speed. Likewise

the expansion waves, which follow the front, are assumed to travel at the same constant speed. Restated, the assumption is simply one of constant shock strength and positive time duration over this increment of space and should be a good assumption for the weaker shock cases and small increments of space. With this model, the following relations are written for the path of a fluid particle starting from $l = 0$ at time $t = 0$:

The velocity of the fluid at t is

$$u = \frac{dl}{dt} \tag{A4}$$

The time required for the fluid to reach l is

$$t = t' + \frac{l}{V_0} \tag{A5}$$

The variation of the fluid velocity with the blast time t' at l is already given by equation (A3). The flow distance l is given by integration of equation (A4) as

$$dl = u(t)dt$$

which is accomplished by first substituting for dt by differentiating equation (A5) and inserting $u(t')$ from equation (A3) and solving for dl to give equation (A4) in nondimensional form as follows:

$$\frac{dl}{V_0 t_d} = \frac{1}{\frac{V_0}{u_2}\frac{e^{\frac{1}{2}\frac{t'}{t_d}}}{1 - \frac{t'}{t_d}} - 1} \, d\left(\frac{t'}{t_d}\right) \tag{A6}$$

Equation (A6) is then integrated to give l as a function of t' and equation (A5) is then substituted into the resulting relation to give l as a function of t. The resulting fluid paths for a few blast-wave overpressures are shown in figure 18 and were obtained by integration of equation (A6) by the method of finite differences.

REFERENCES

1. Bleakney, Walker: The Diffraction of Shock Waves Around Obstacles and the Transient Loading of Structures. Tech. Rep. II-3 (Contract N6ori-105), Princeton Univ., Dept. Phys., Mar. 16, 1950.

2. Uhlenbeck, George: Diffraction of Shock Waves Around Various Obstacles. Rep. 50-1 (Contract No. N6-ONR-232), Univ. of Michigan, Eng. Res. Inst., Mar. 21, 1950.

3. Bingham, Harry H., Weimer, David K., and Griffith, Wayland: The Cylinder and Semicylinder in Subsonic Flow. Tech. Rep. II-13 (Contract N6ori-105), Dept, Phys., Princeton Univ., July 1952.

4. Turner, Eugene B., Johnson, Walter R., et al.: Diffraction of a Mach Stem Shock Over a Square Block. Rep. No. AFSWP-704, Project 2241 (Contract No. Nonr-1224(04)), Eng. Res. Inst., Univ. of Michigan, Jan. 1956.

5. Howard, L. N., and Matthews, D. L.: On the Vortices Produced in Shock Diffraction. Tech. Rep. II-21 (Contract N6ori-105), Princeton Univ., Dept. Phys, July 1955.

6. Rott, Nicholas: Diffraction of a Weak Shock With Vortex Generation. Jour. Fluid Mechanics, vol. 1, pt. 1, May 1956, pp. 111-128.

7. Liggins, M. Lorraine: Transient Drag and Its Effect on Structures. Vol. II - Bibliography to Final Report. MR 1013 (Contract No. AF 33(616)-2285), Am. Machine & Foundry Co., Feb. 24, 1955.

8. Beichler, Glenn P.: Records of Air Shock Loading On a Three Dimensional Model. Tech. Note No. 842, Ballistic Res. Labs., Aberdeen Proving Ground, Jan. 1954.

9. Anon.: Blast Effects on Buildings and Structures - Operation of Six-Foot and Two-Foot Shock Tubes. Effect of Long Versus Short Duration Blast Loadings on Structures. Rep. No. 18 (Final Test Rep. No. 1; Contract No. AF 33(616)-2644), Armour Res. Foundation, Illinois Inst. Tech., Aug. 22, 1955. (Also available from ASTIA as AD No. 72567.)

10. Huber, Paul W., and McFarland, Donald R.: Boundary-Layer Growth and Shock Attenuation in a Shock Tube With Roughness. NACA TN 3627, 1956.

11. Armendt, B. F., Smith, R., and Wise, R. C.: The Initial Decay of Pressure Behind a Shock Front: Comparison of Experimental and Calculated Results. Memo. Rep. No. 997, Ballistic Res. Labs., Aberdeen Proving Ground, Apr. 1956.

12. Curtis, Wesley: Free Air Blast Measurements on Spherical Pentolite. Memo. Rep. No. 544, Ballistic Res. Labs., Aberdeen Proving Ground, July 1951.

TABLE I

COMPARISON OF MODELS AND TEST CONDITIONS

Model	Model shape	Height, in.	Length, in.	Corner radius, in.
1	Square	0.25	6.00	0.001 ± 0.001
2	Square	.25	6.00	0.016 ± 0.002
3	Square	.25	2.00	0.016 ± 0.002
4	Half round	.25	6.00	0.25 ± 0.01

Peak overpressure of blast, lb/sq in. 4.0
Positive time duration, μsec 900
Blast front velocity, ft/sec 1,260
Peak blast flow velocity, ft/sec 198

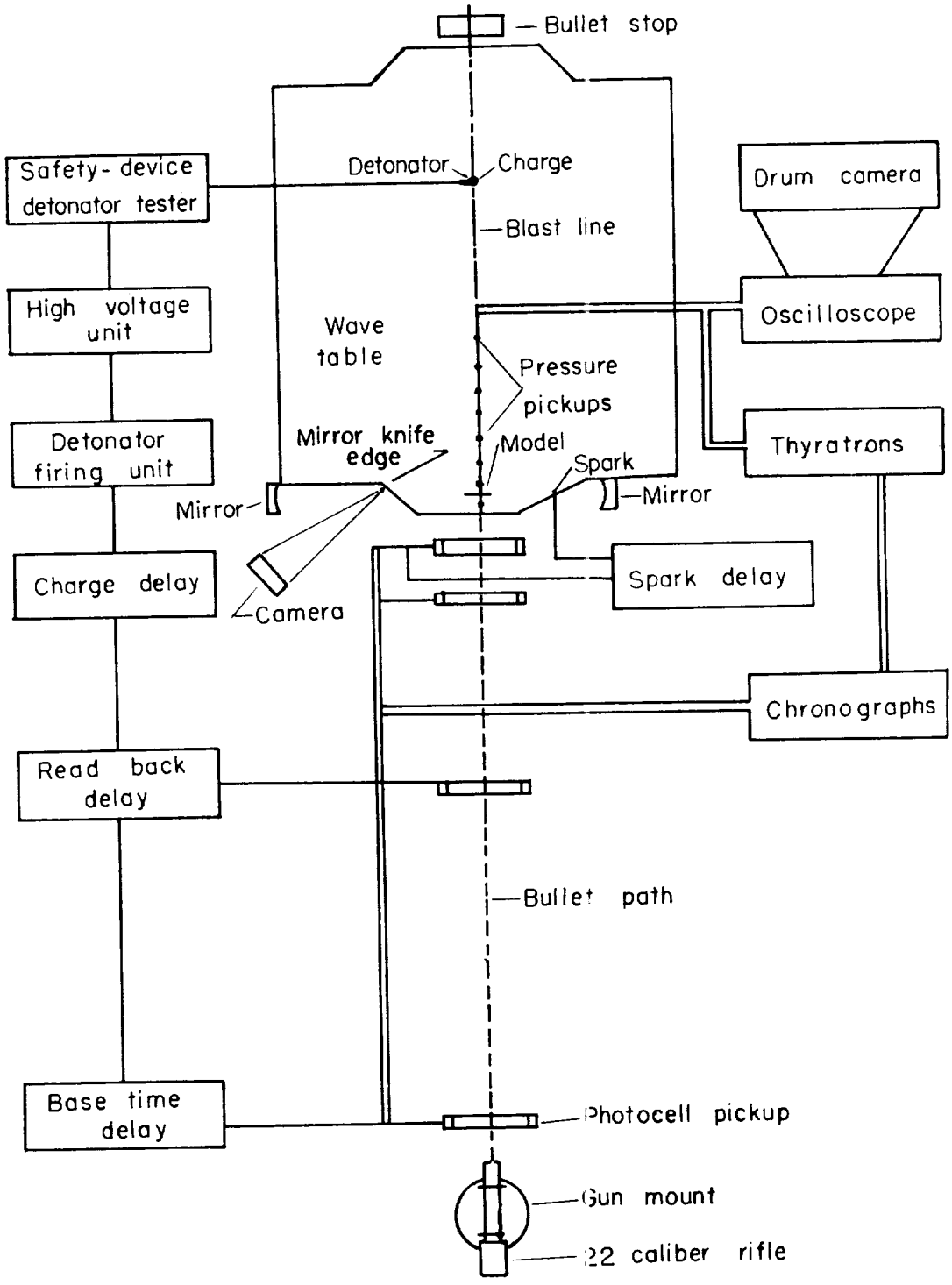

Figure 1.- Schematic diagram of wave-table setup.

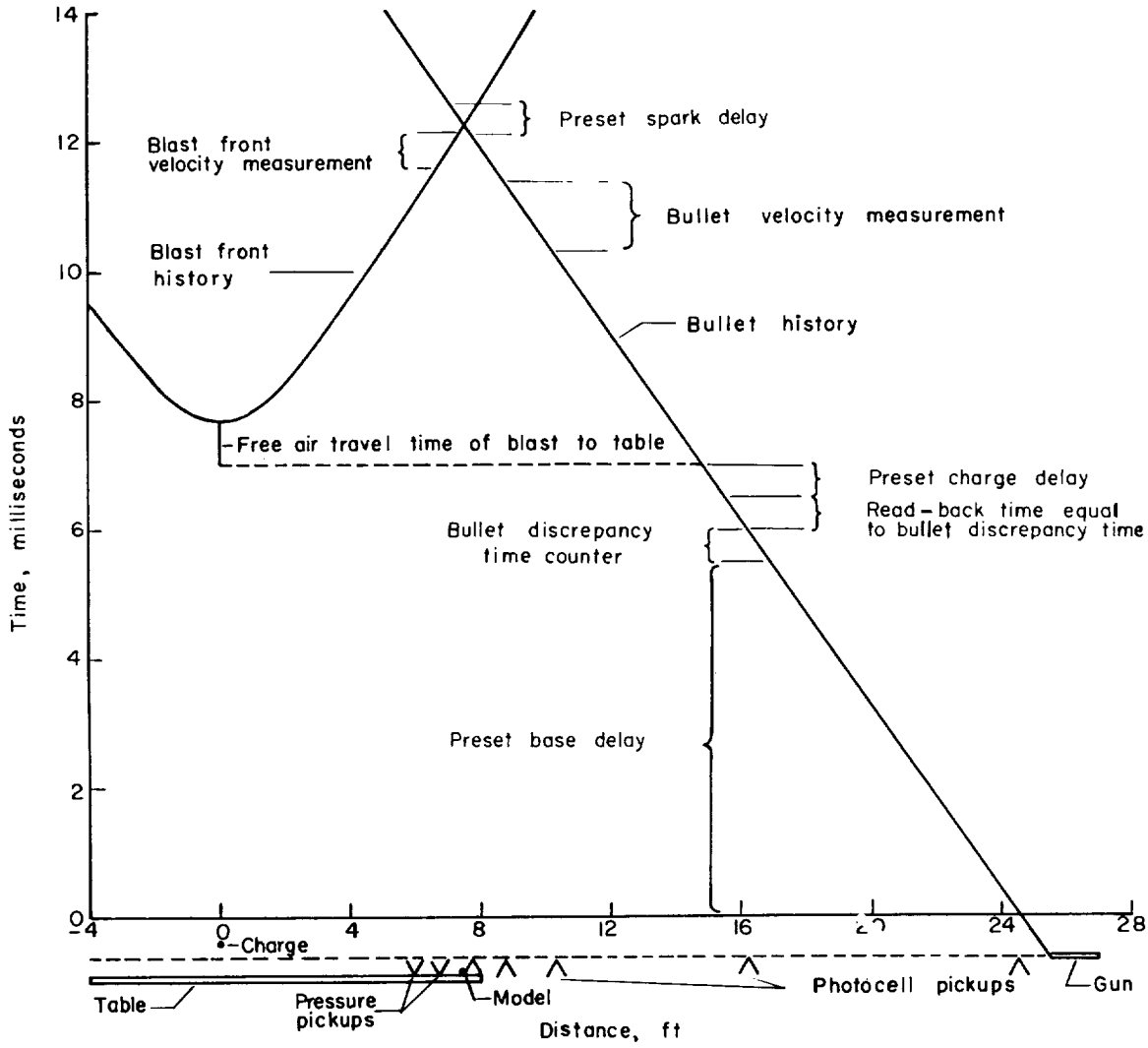

Figure 2.- A position-time sequence of wave-table events.

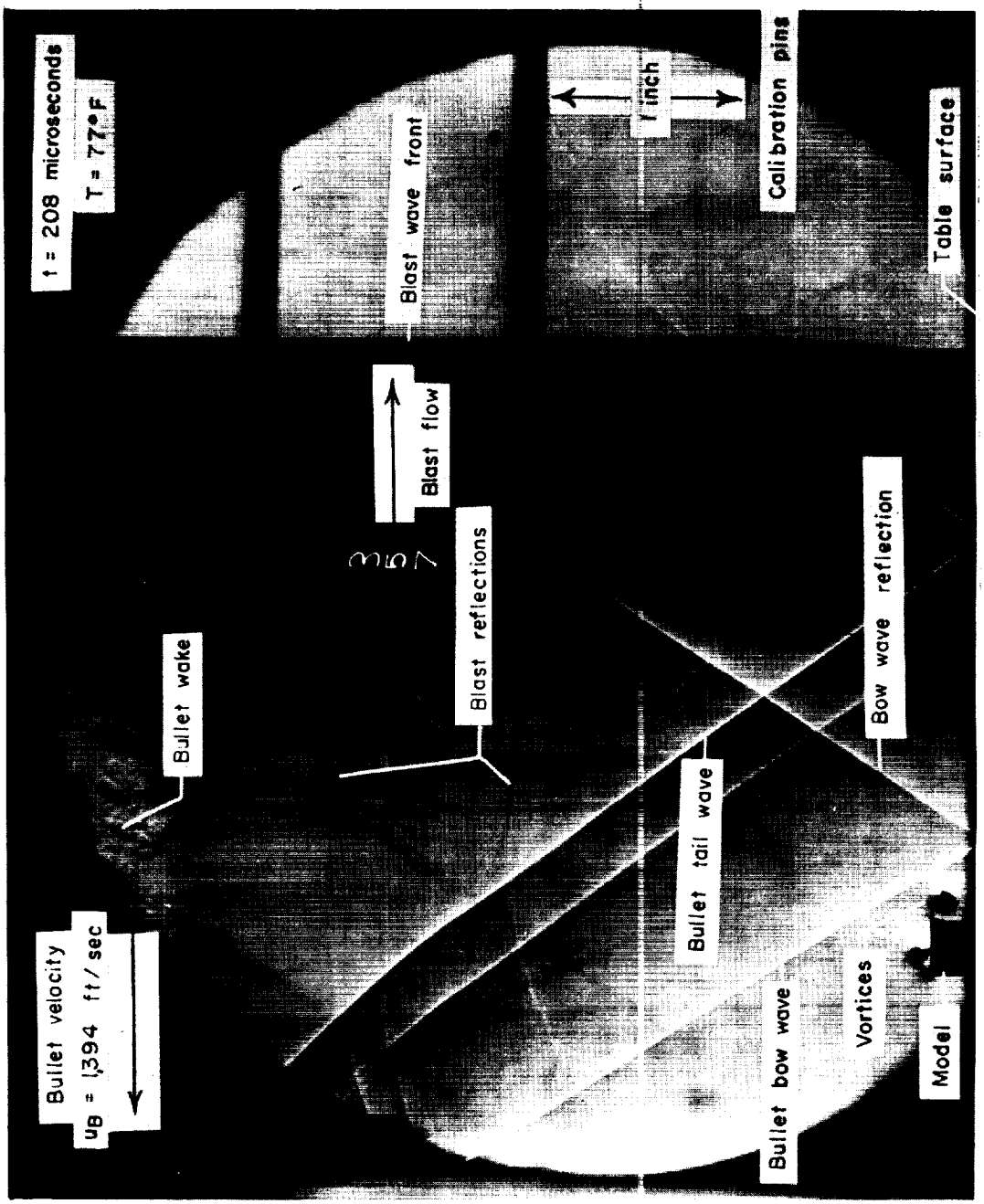

Figure 3.- A typical schlieren photograph. L-58-2561

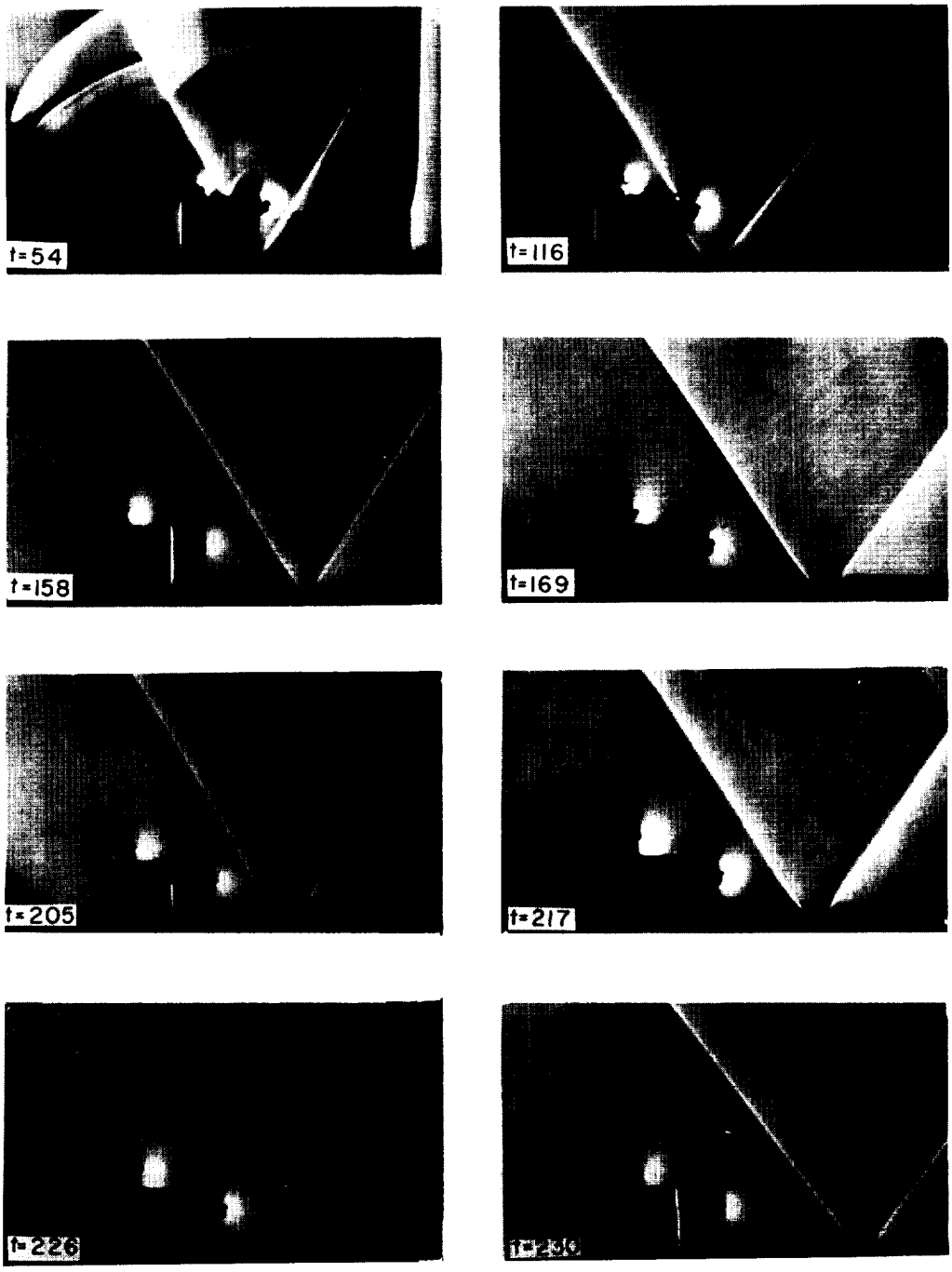

L-58-2562

Figure 4.- A sequence of schlieren photographs of model 1 (1/4-inch ground square bar, 6 inches long). Time t is given in microseconds. Each photograph represents one test.

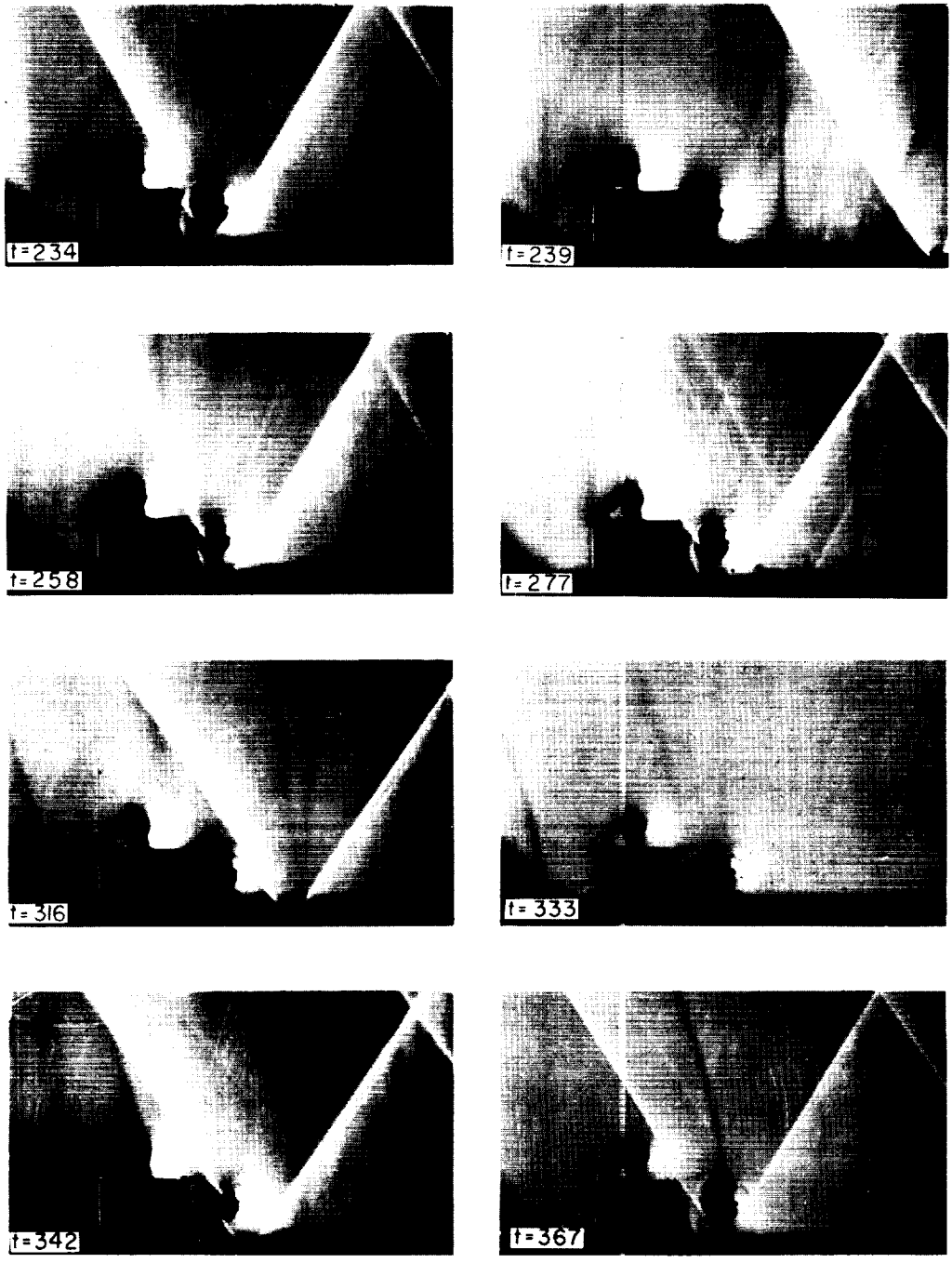

Figure 4.- Continued. L-58-2563

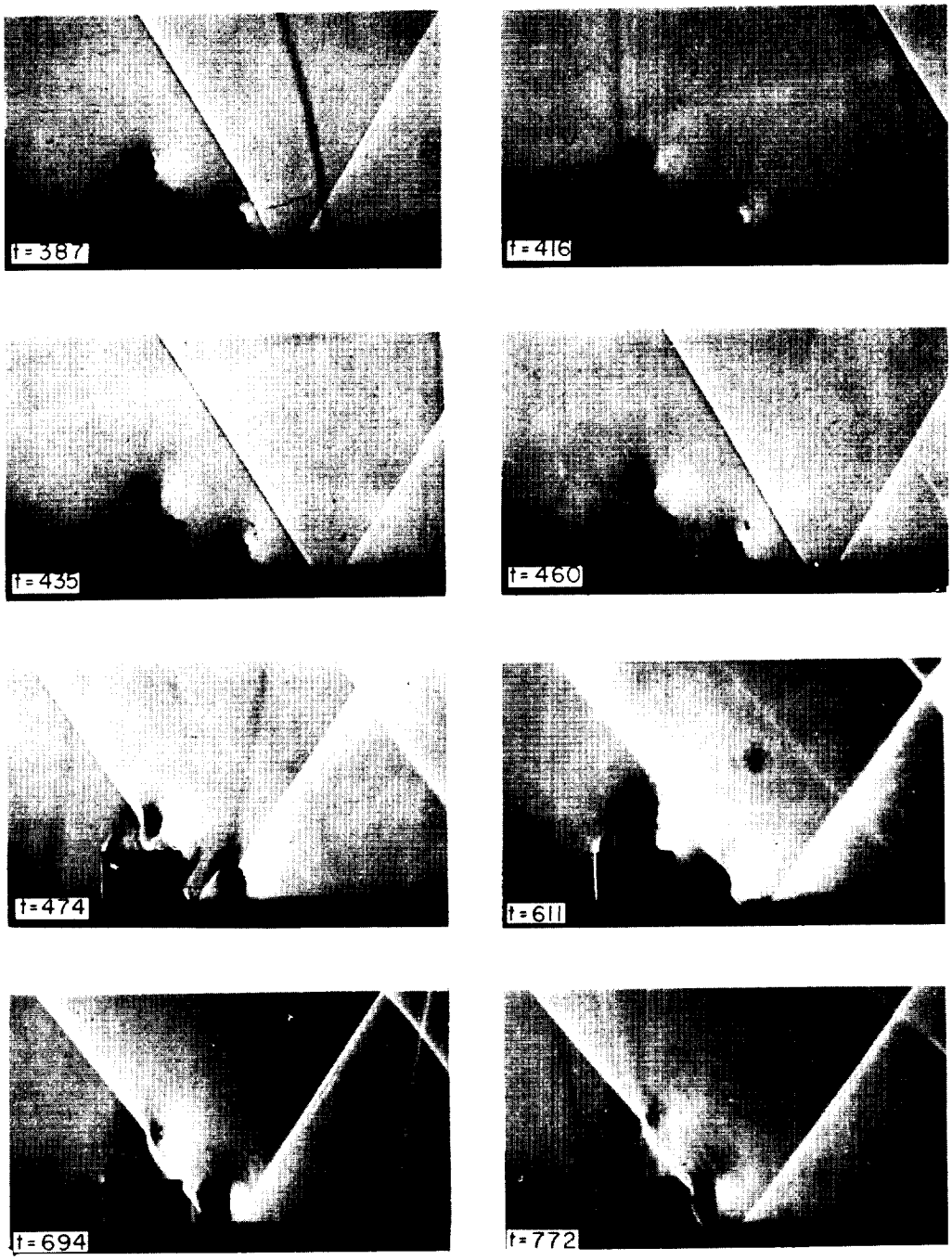

Figure 4.- Concluded. L-58-2564

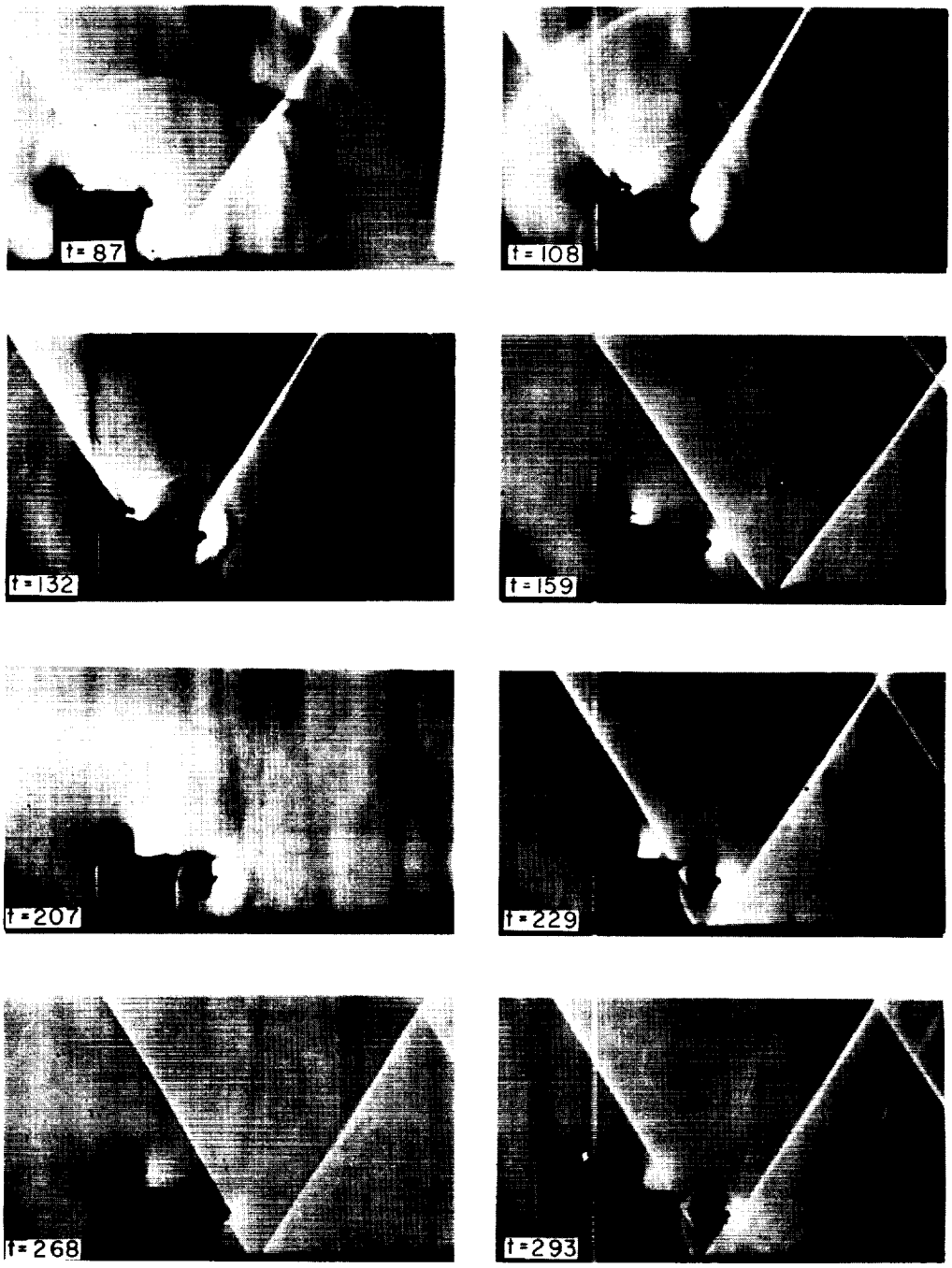

L-58-2565

Figure 5.- A sequence of schlieren photographs of model 2 (1/4-inch regular square bar stock, 6 inches long). Time t is given in microseconds. Each photograph represents one test.

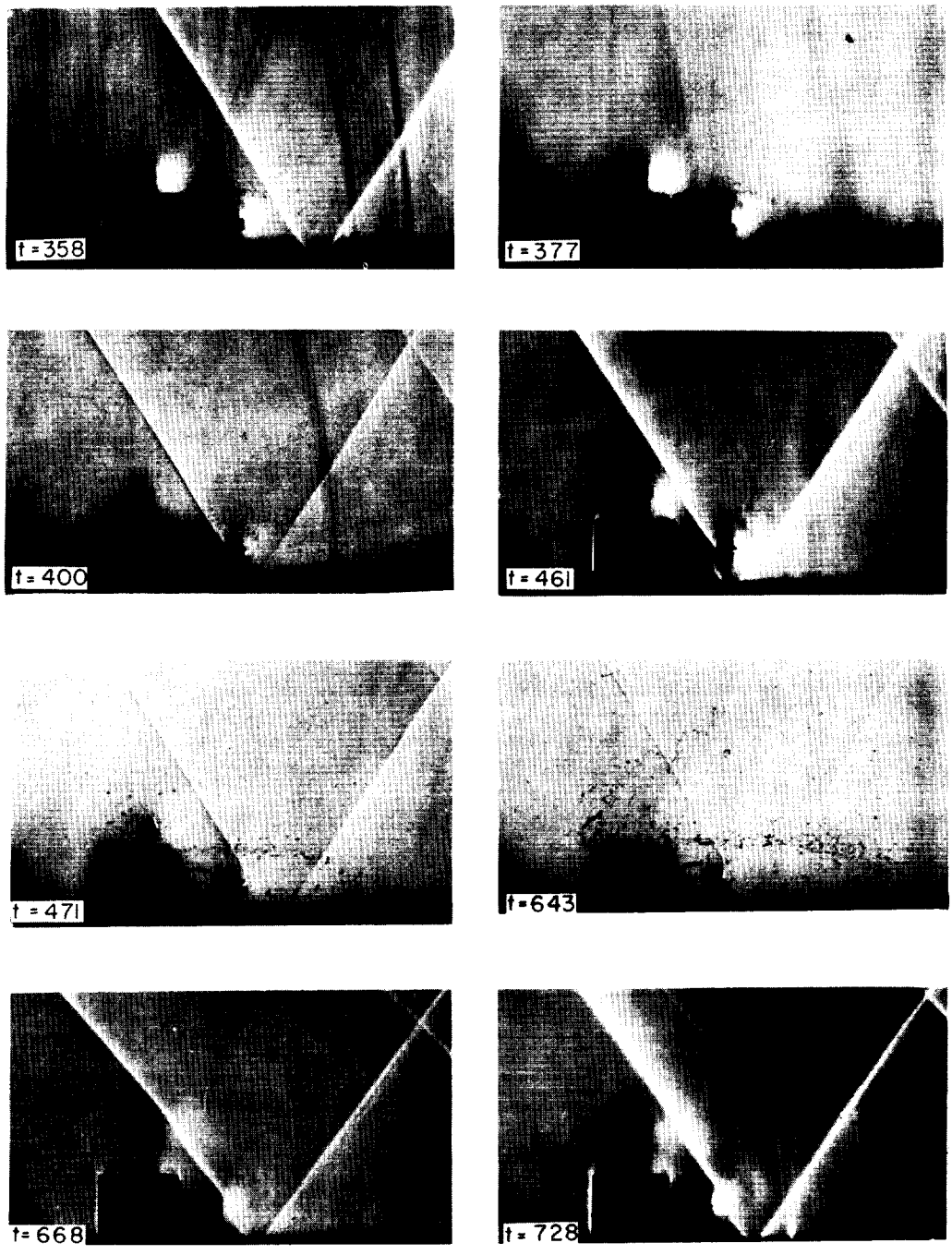

Figure 5.- Concluded. L-58-2566

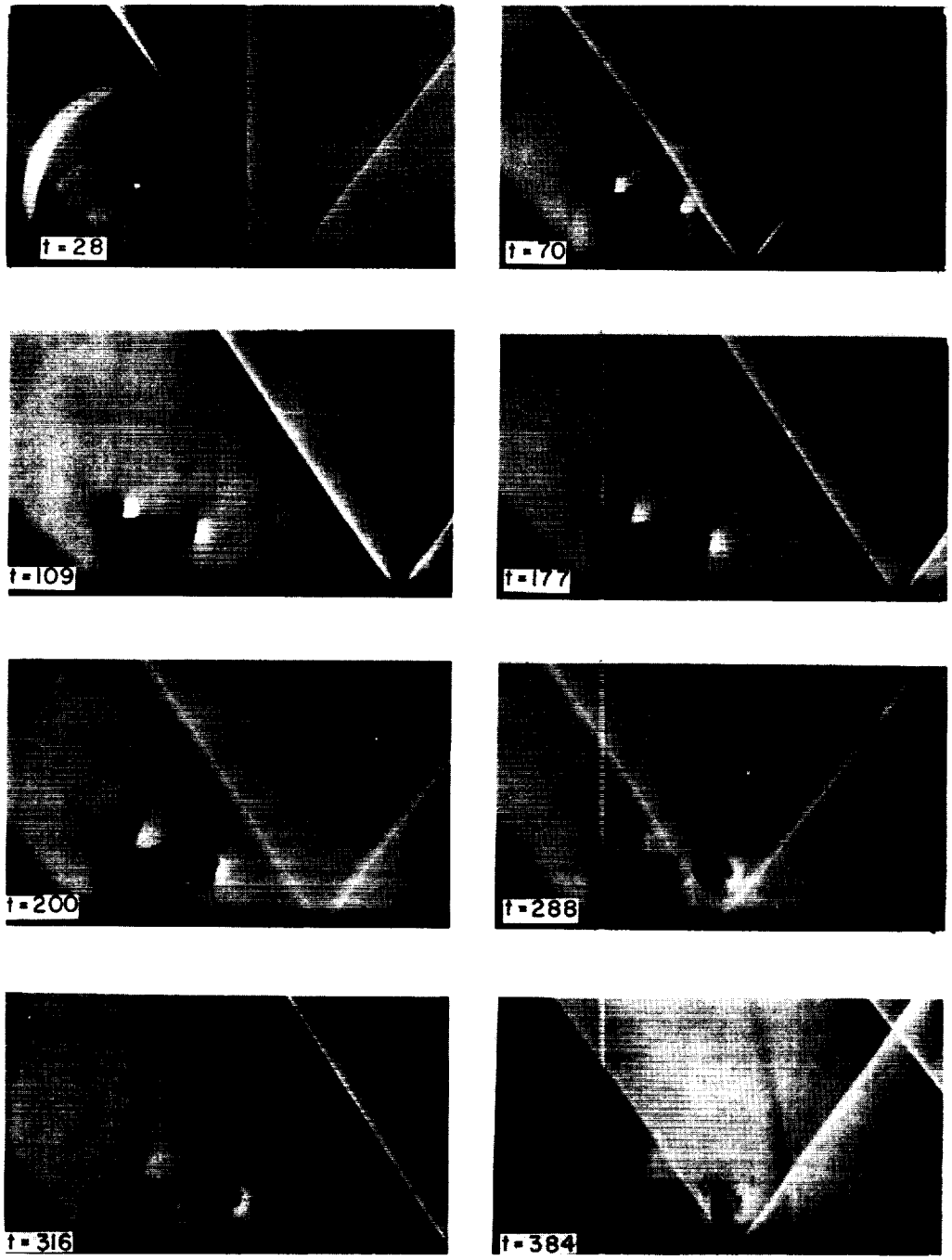

L-58-2567

Figure 6.- A sequence of schlieren photographs of model 3 (1/4-inch regular bar stock, 2 inches long). Time t is given in microseconds. Each photograph represents one test.

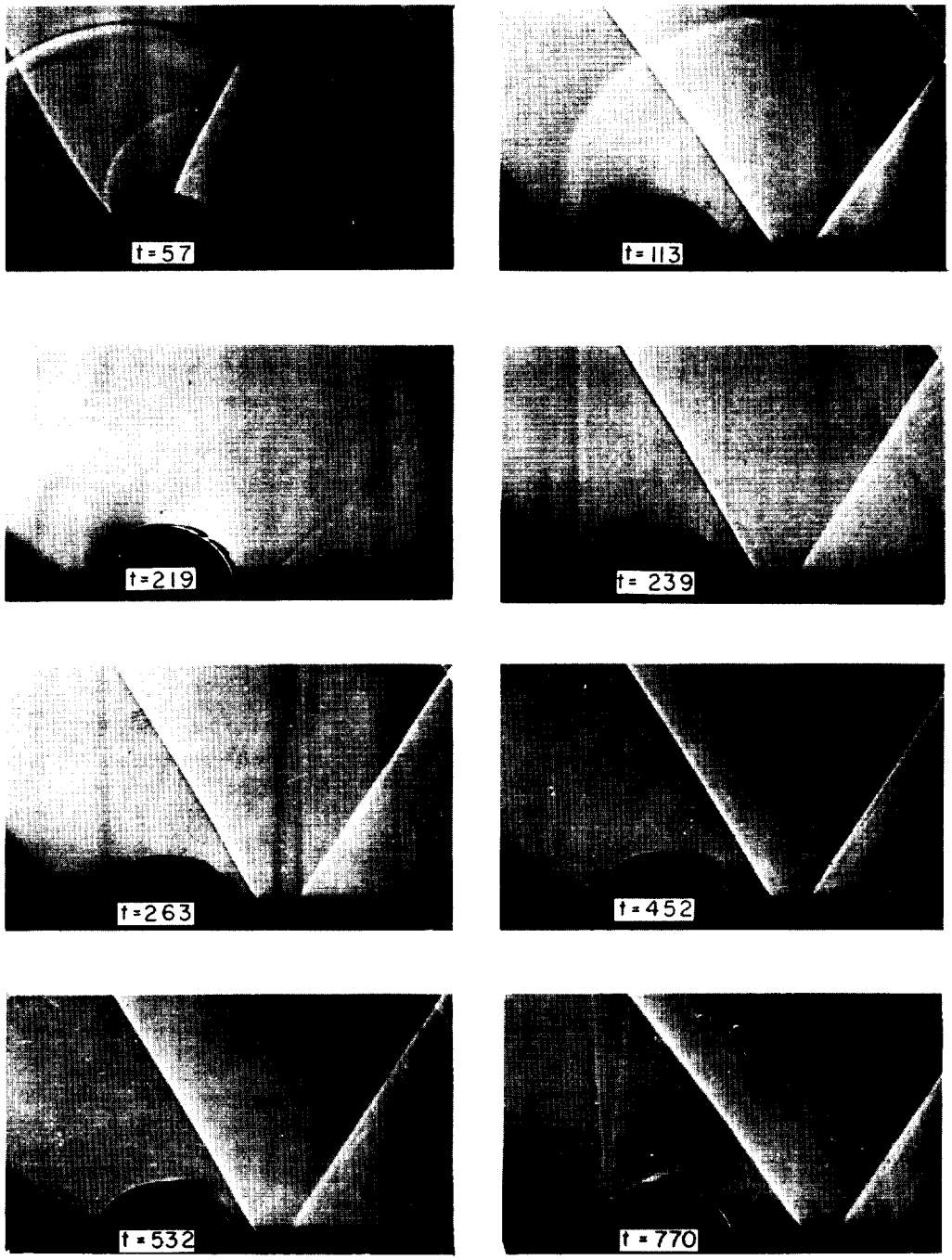

L-58-2568

Figure 7.- A sequence of schlieren photographs of model 4 (1/4-inch-radius half-round brass bar, 6 inches long). Time t is given in microseconds. Each photograph represents one test.

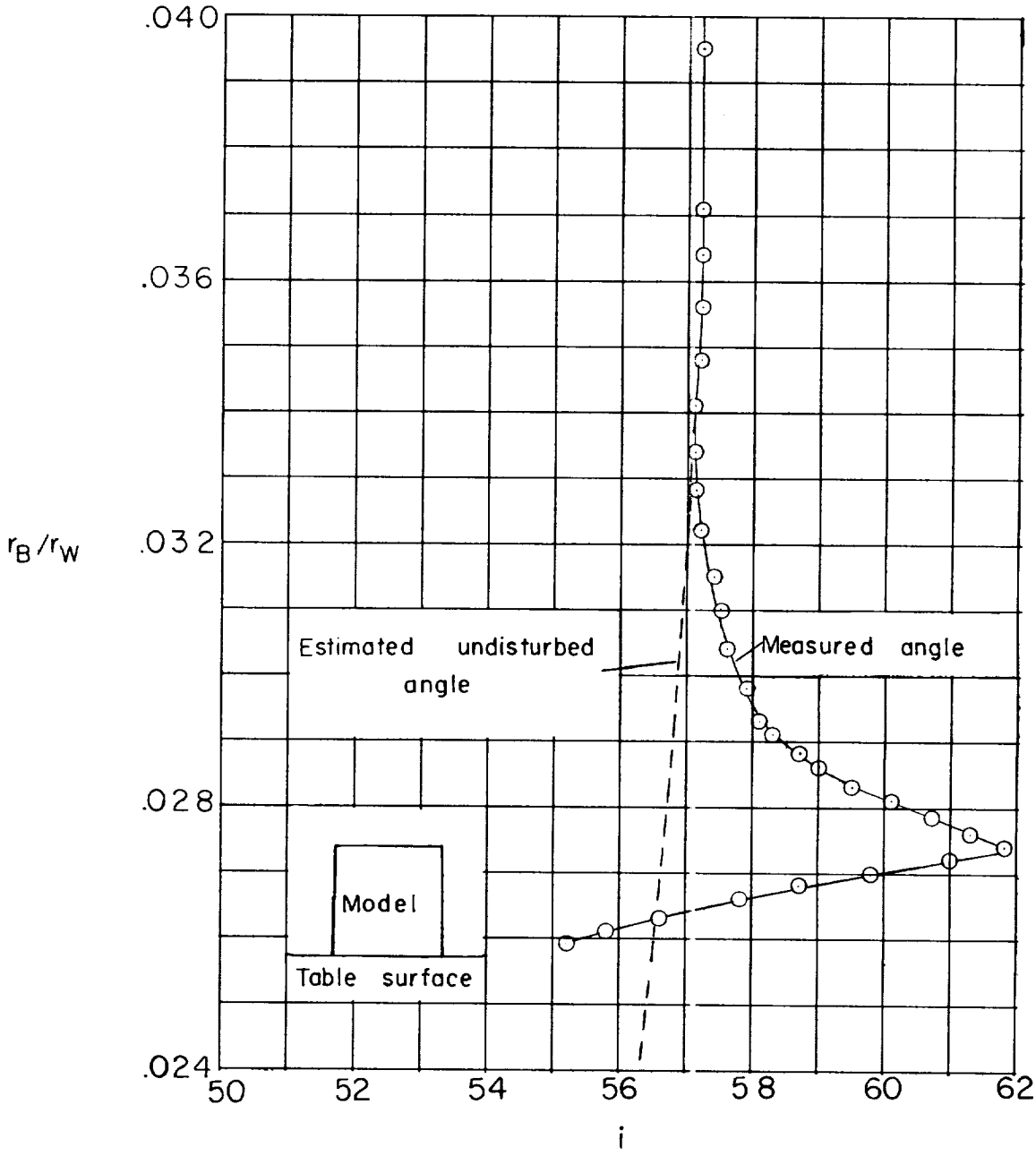

Figure 8.- Bullet bow-wave distortion due to velocity field about a body in the blast-induced flow as shown in figure 3.

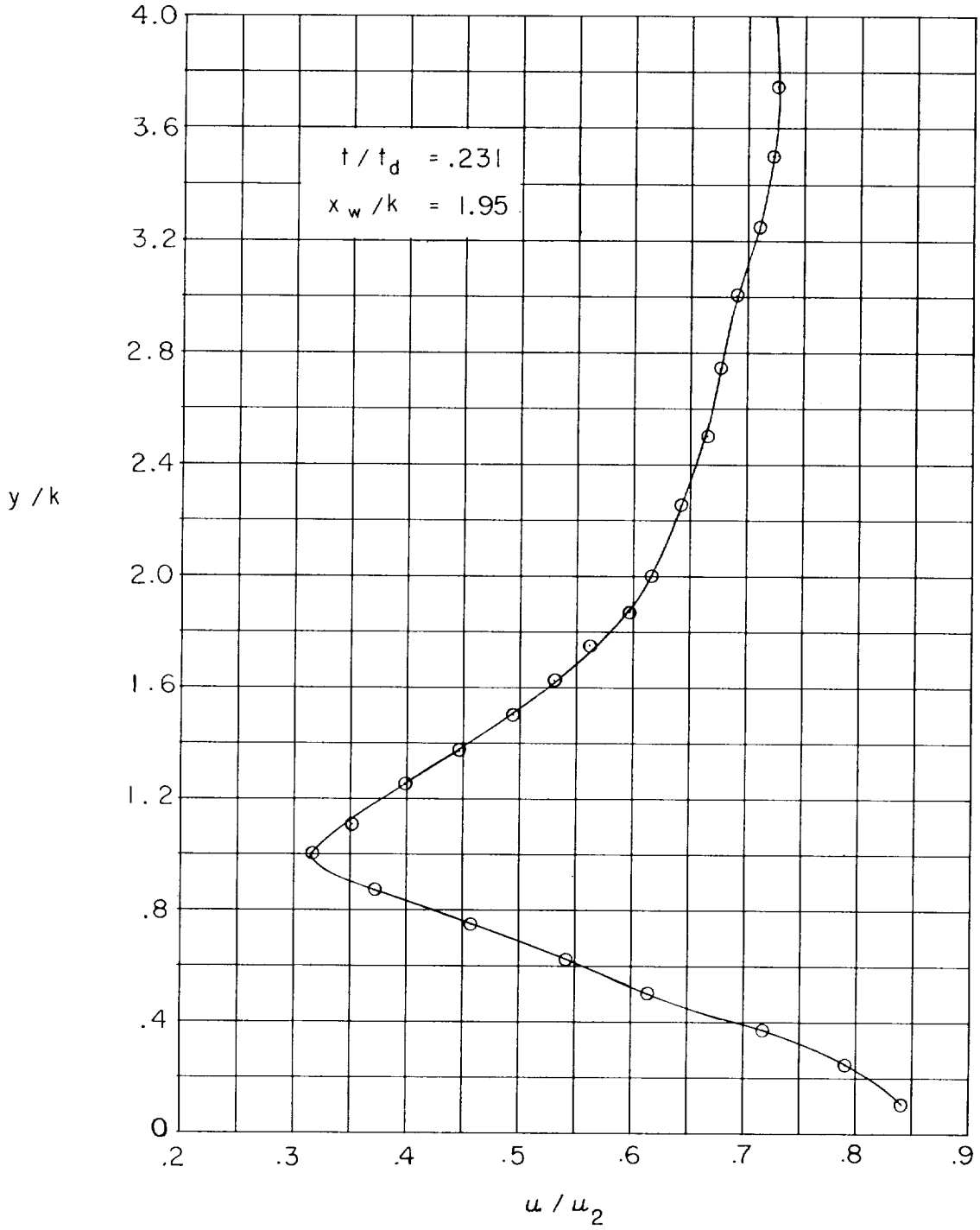

Figure 9.- Velocity variation along a bullet bow wave in the blast-induced flow field about a body for the data shown in figure 8.

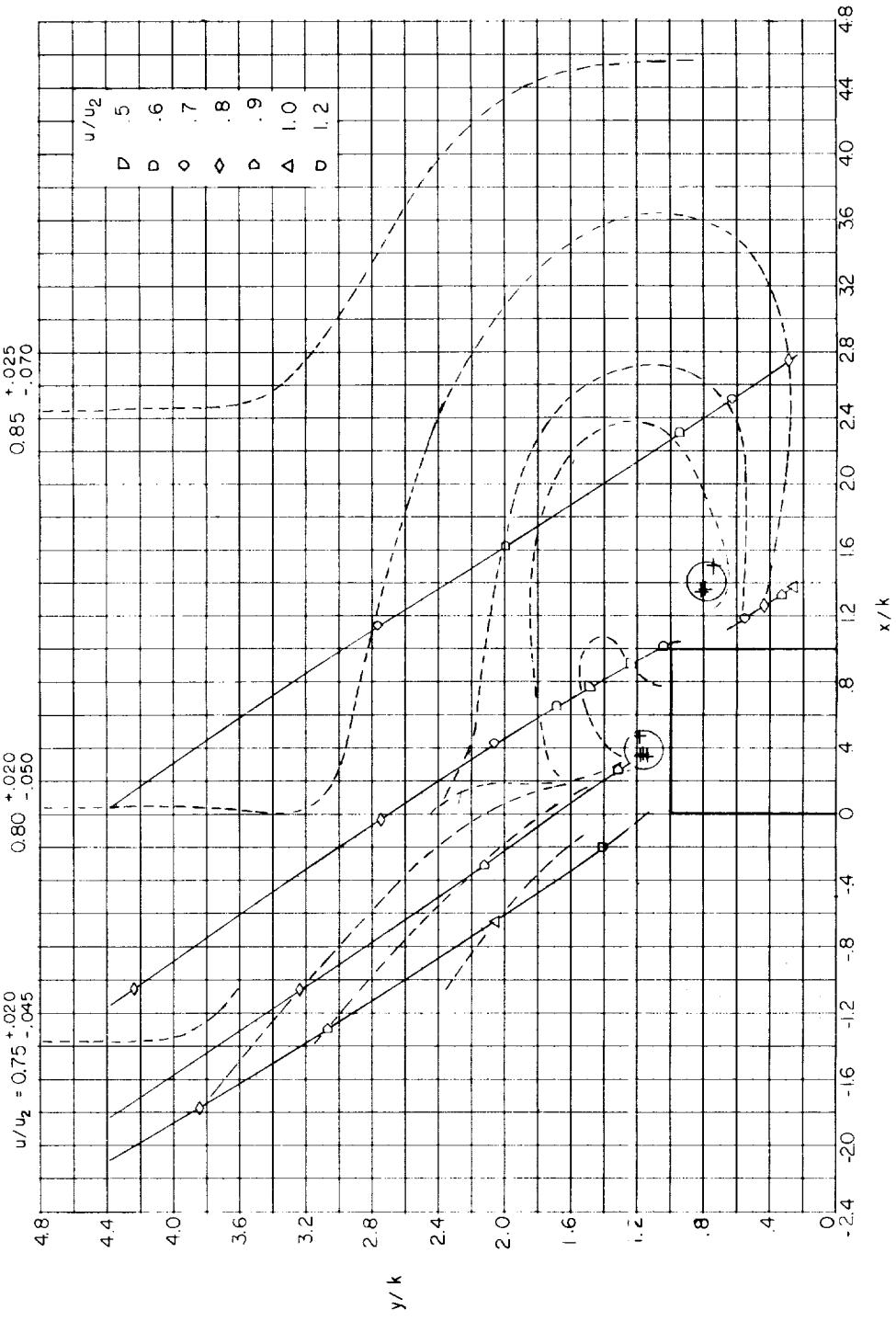

(a) Flow times t/t_d from 0.13 to 0.19.

Figure 10.- Composite of velocity measurements showing velocity contours for model 1. The crossmark + indicates the center of each vortex.

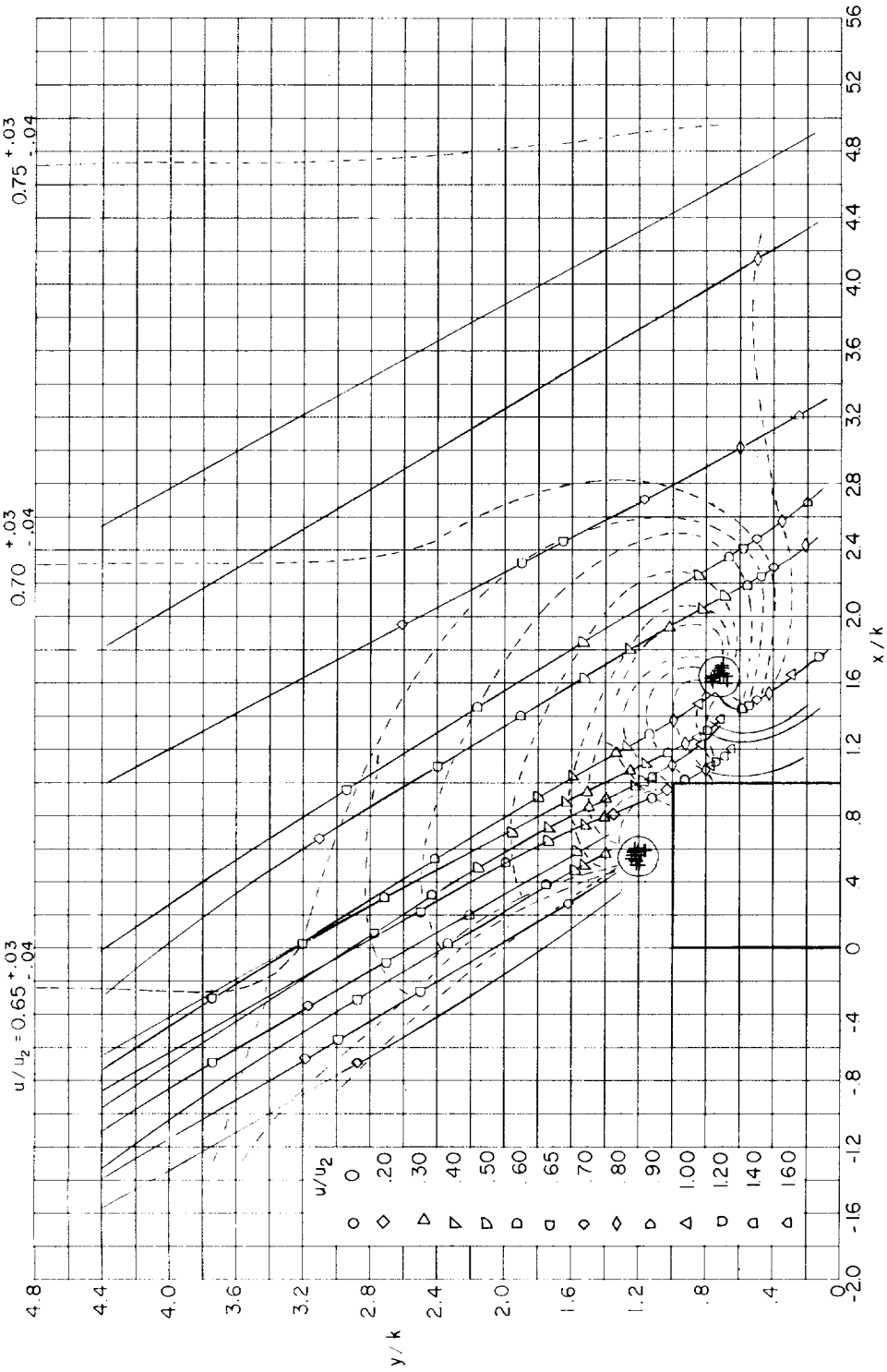

(b) Flow times t/t_d from 0.23 to 0.29.

Figure 10.- Continued.

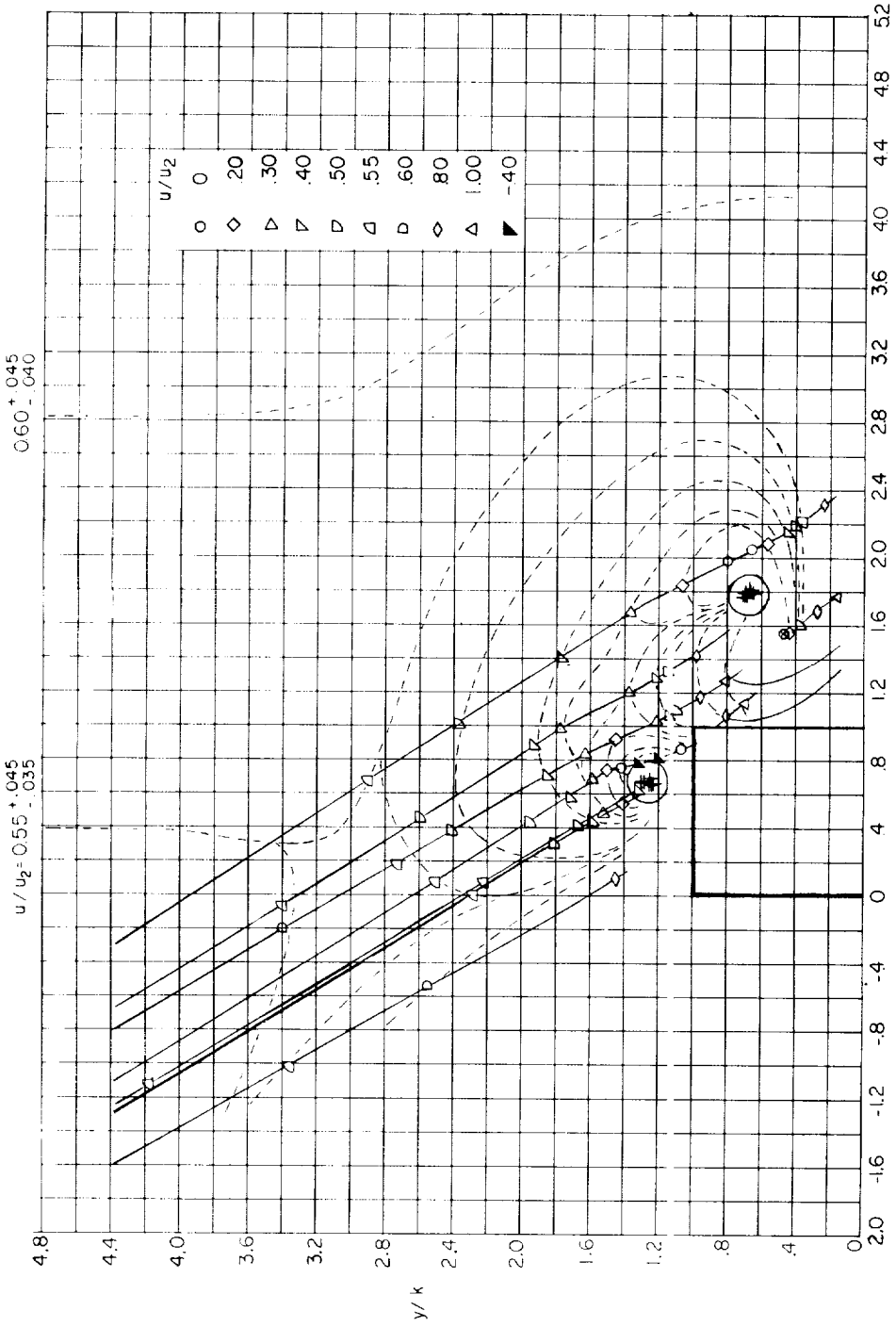

(c) Flow times t/t_d from 0.31 to 0.38.

Figure 10.- Continued.

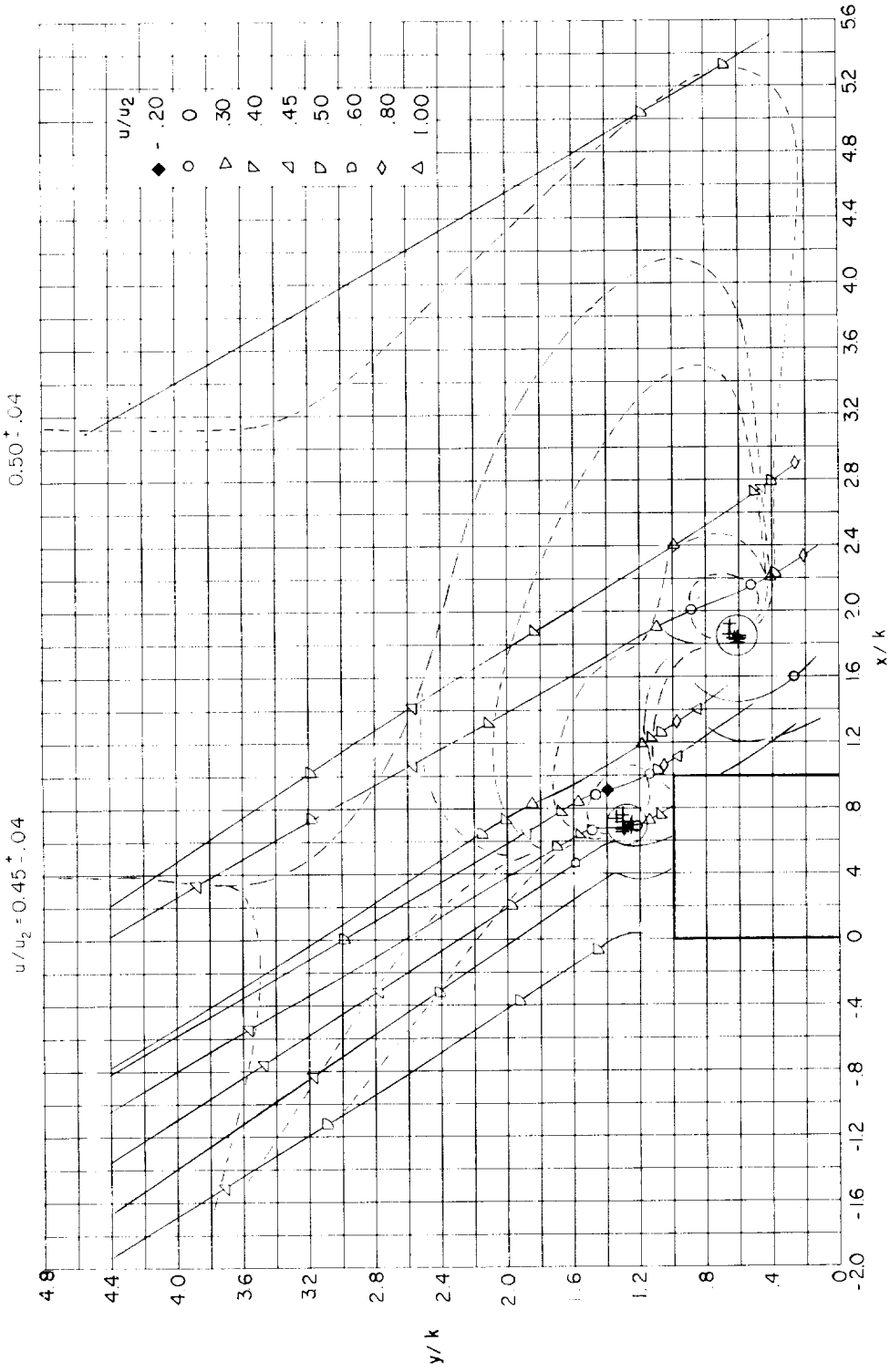

(d) Flow times t/t_d from 0.40 to 0.48.

Figure 10.- Continued.

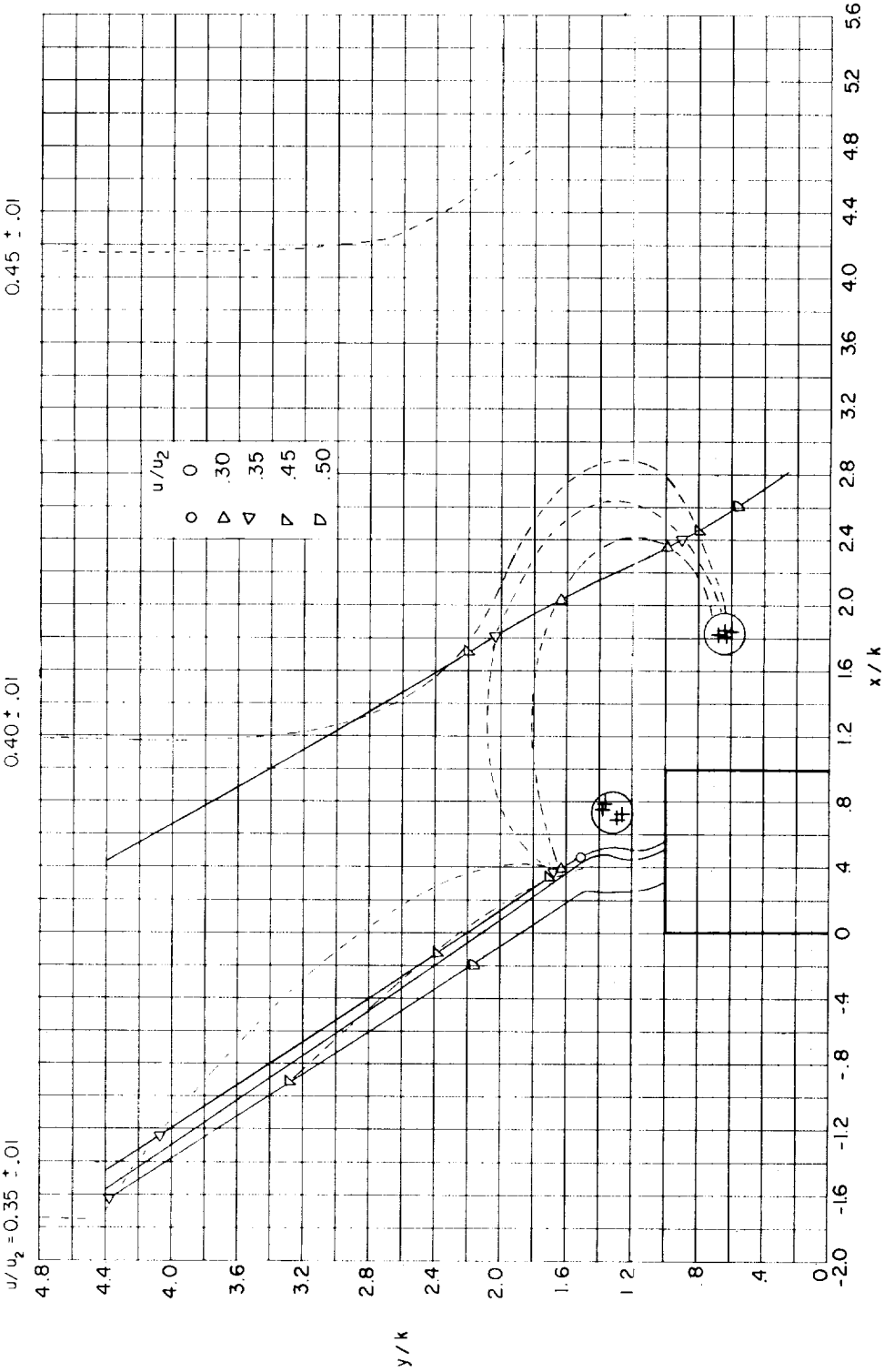

(e) Flow times t/t_d from 0.50 to 0.53.

Figure 10.- Concluded.

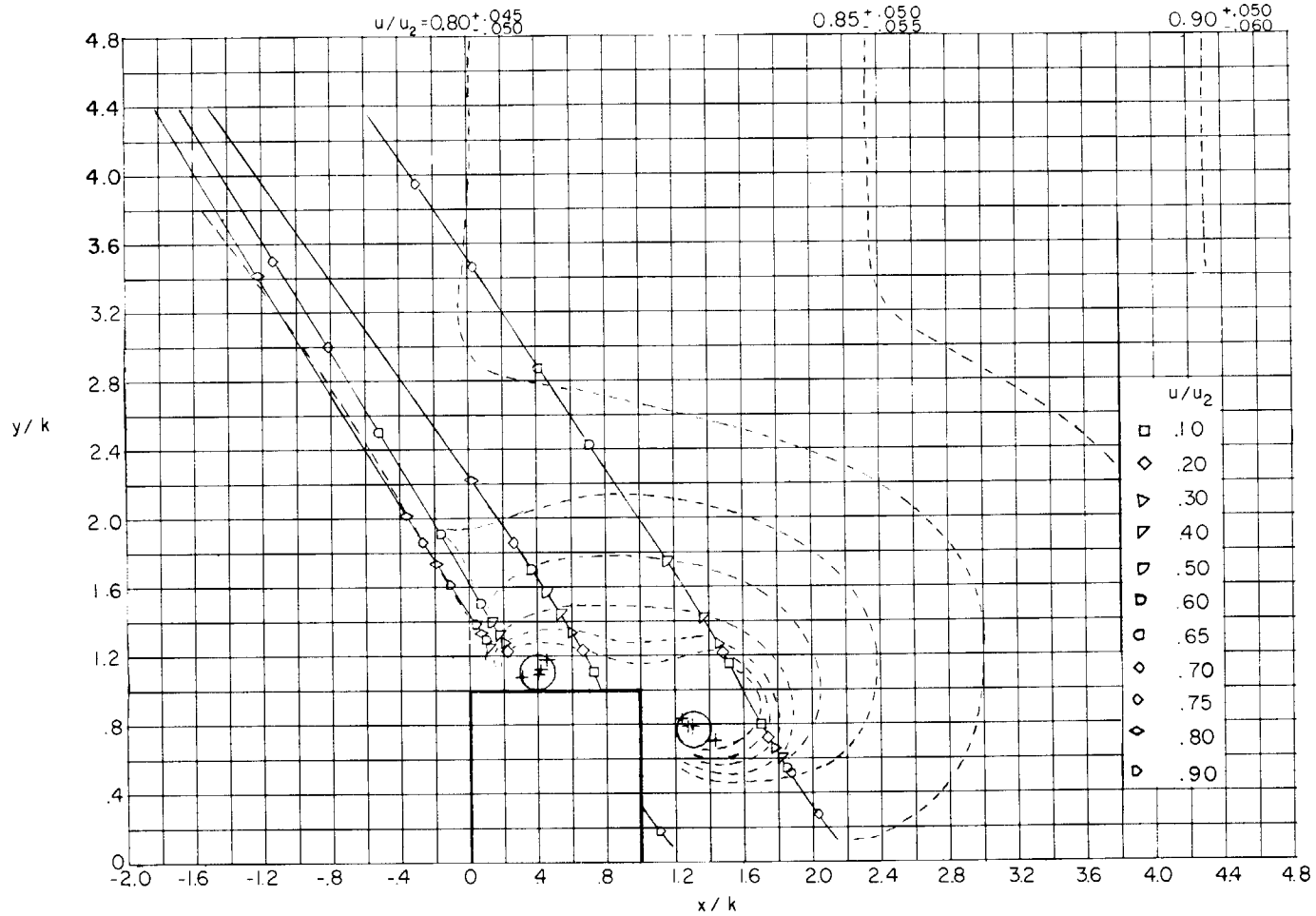

(a) Flow times t/t_d from 0.10 to 0.18.

Figure 11.- Composite of velocity measurements showing velocity contours for model 2. The crossmark + indicates the center of each vortex.

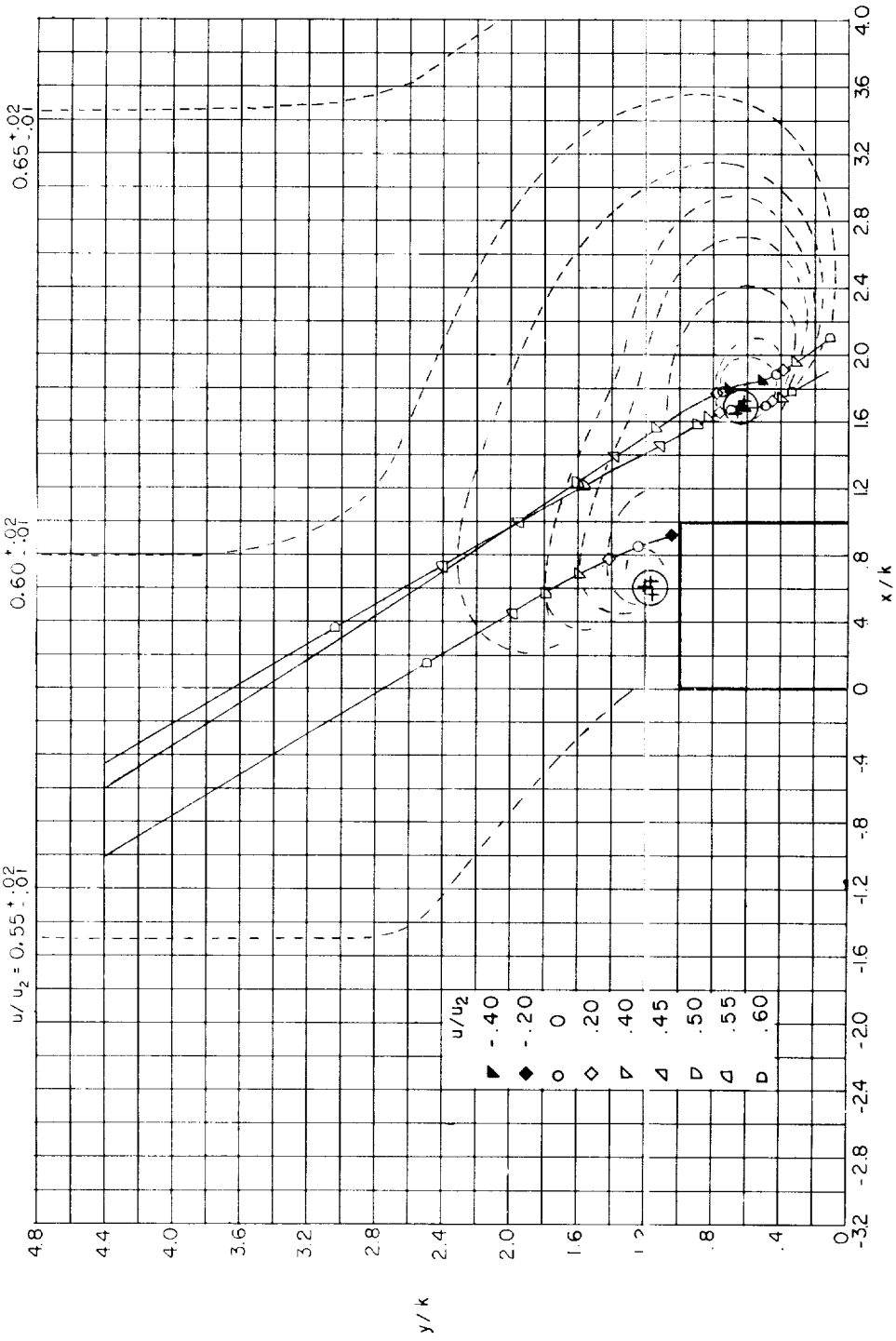

(b) Flow times t/t_d from 0.30 to 0.33.

Figure 11.- Continued.

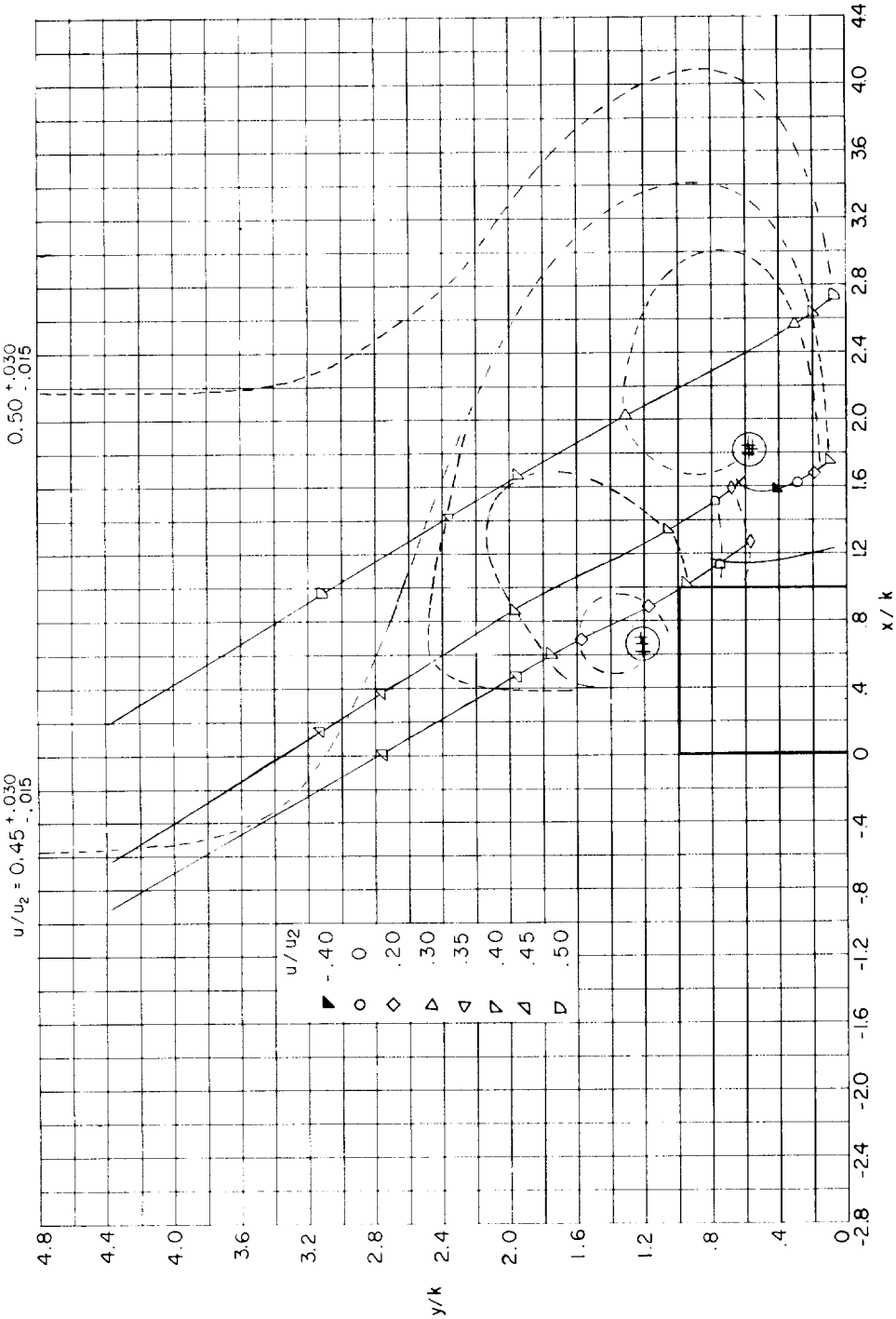

(c) Flow times t/t_d from 0.40 to 0.44.

Figure 11.- Continued.

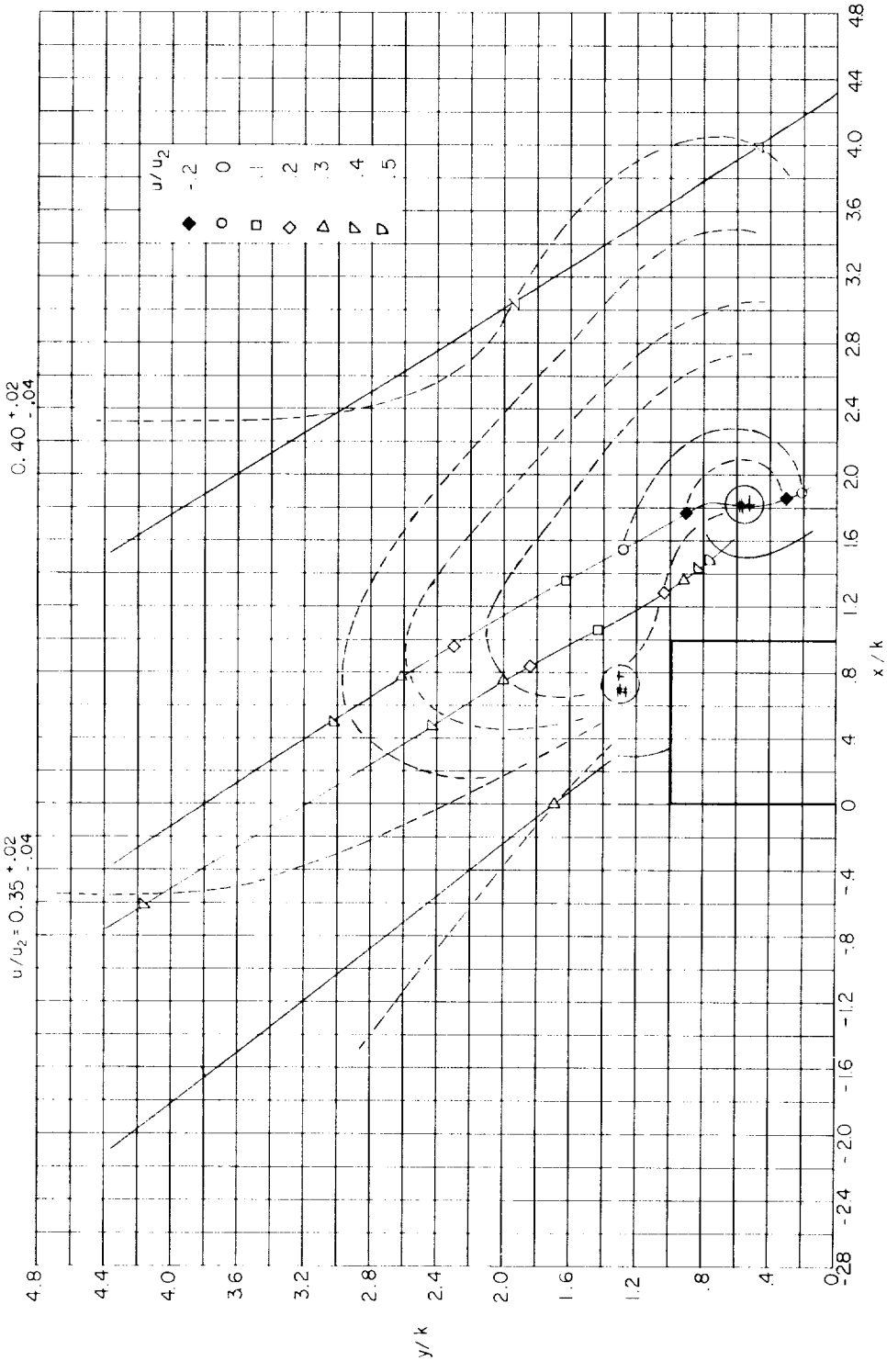

(d) Flow times t/t_d from 0.51 to 0.58.

Figure 11.- Concluded.

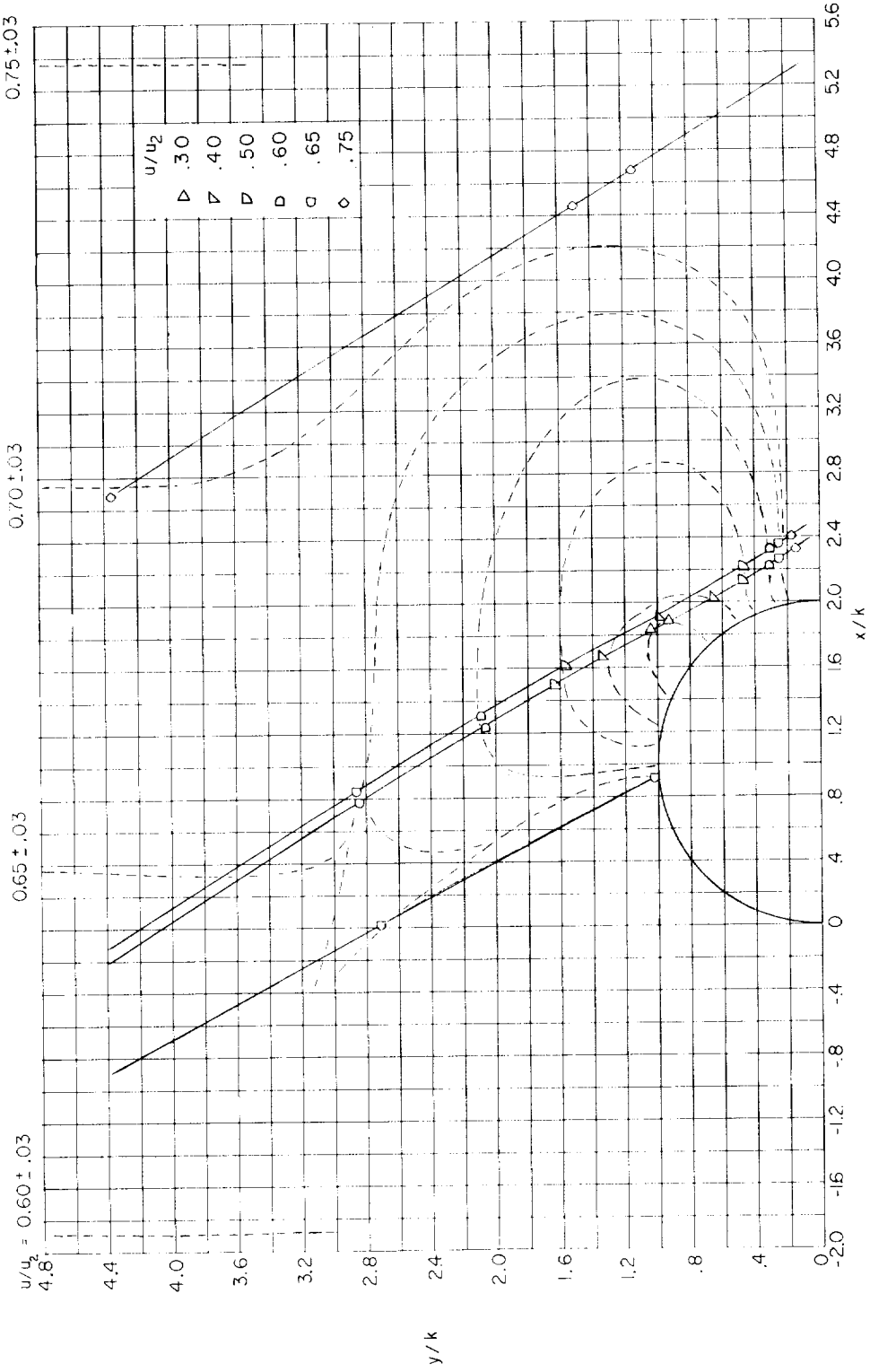

(a) Flow times t/t_d from 0.24 to 0.29.

Figure 12.- Composite of velocity measurements showing velocity contours for model 4.

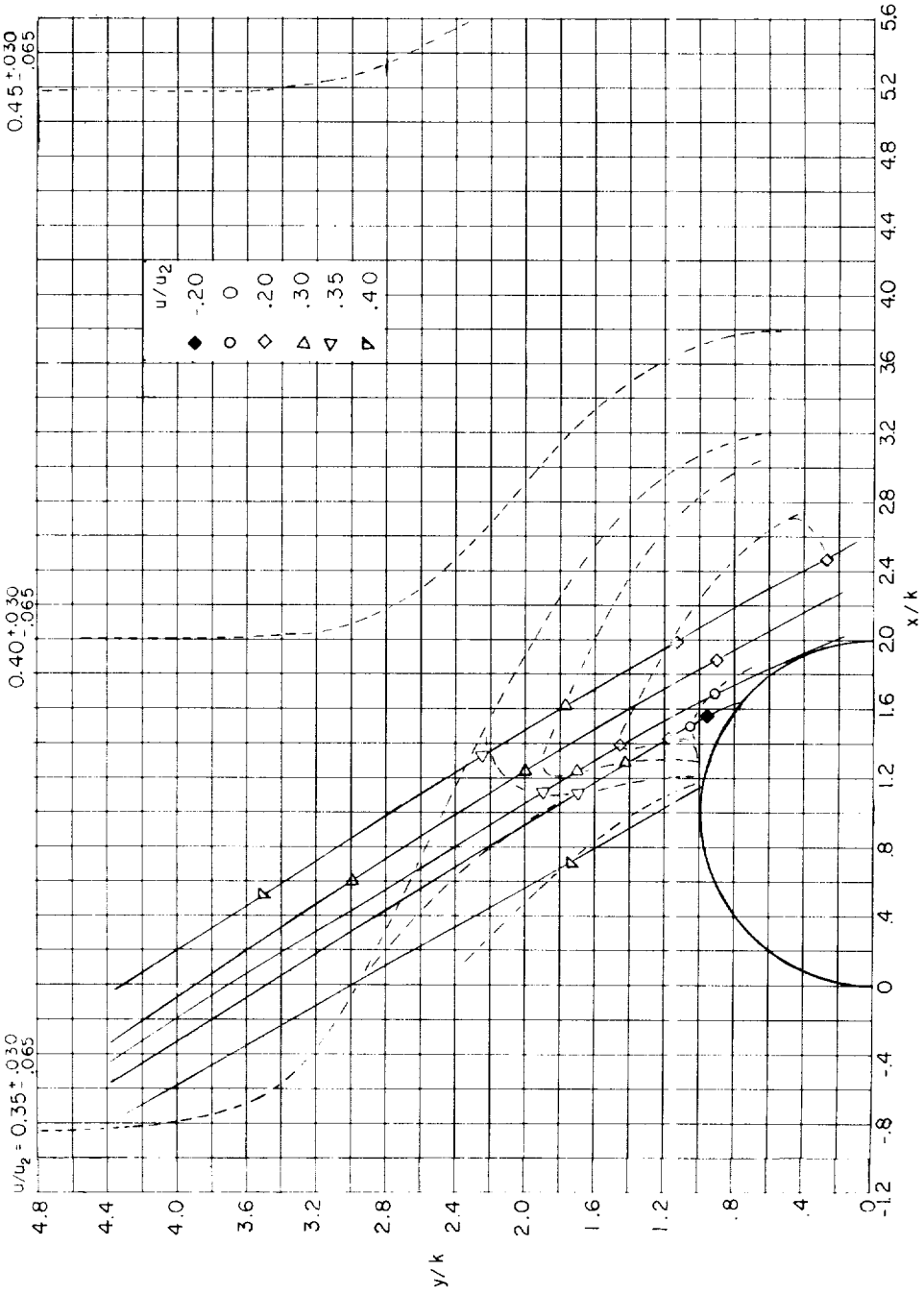

(b) Flow times t/t_d from 0.49 to 0.59.

Figure 12.- Concluded.

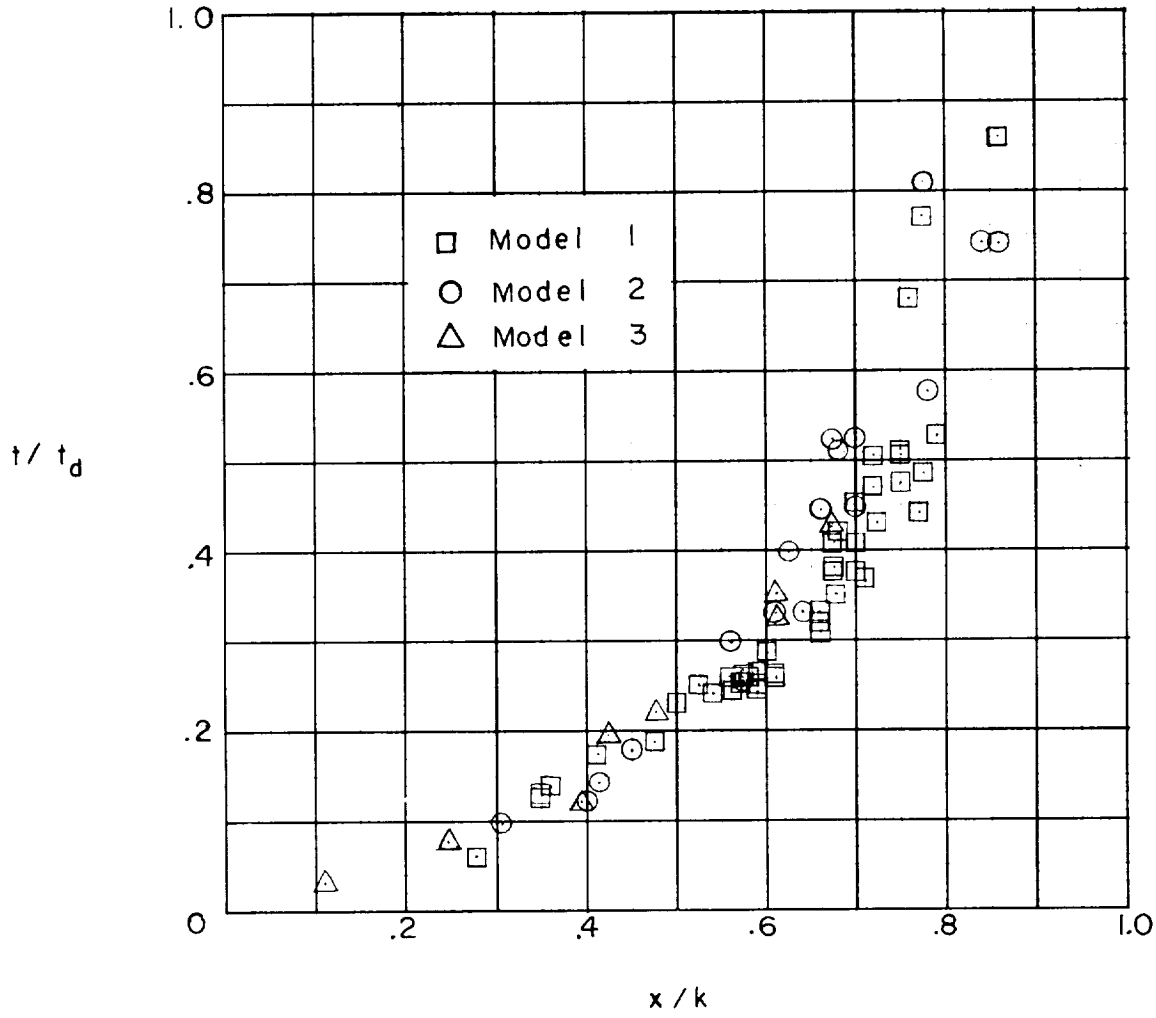

Figure 13.- Horizontal component of leading-edge vortex movement with time.

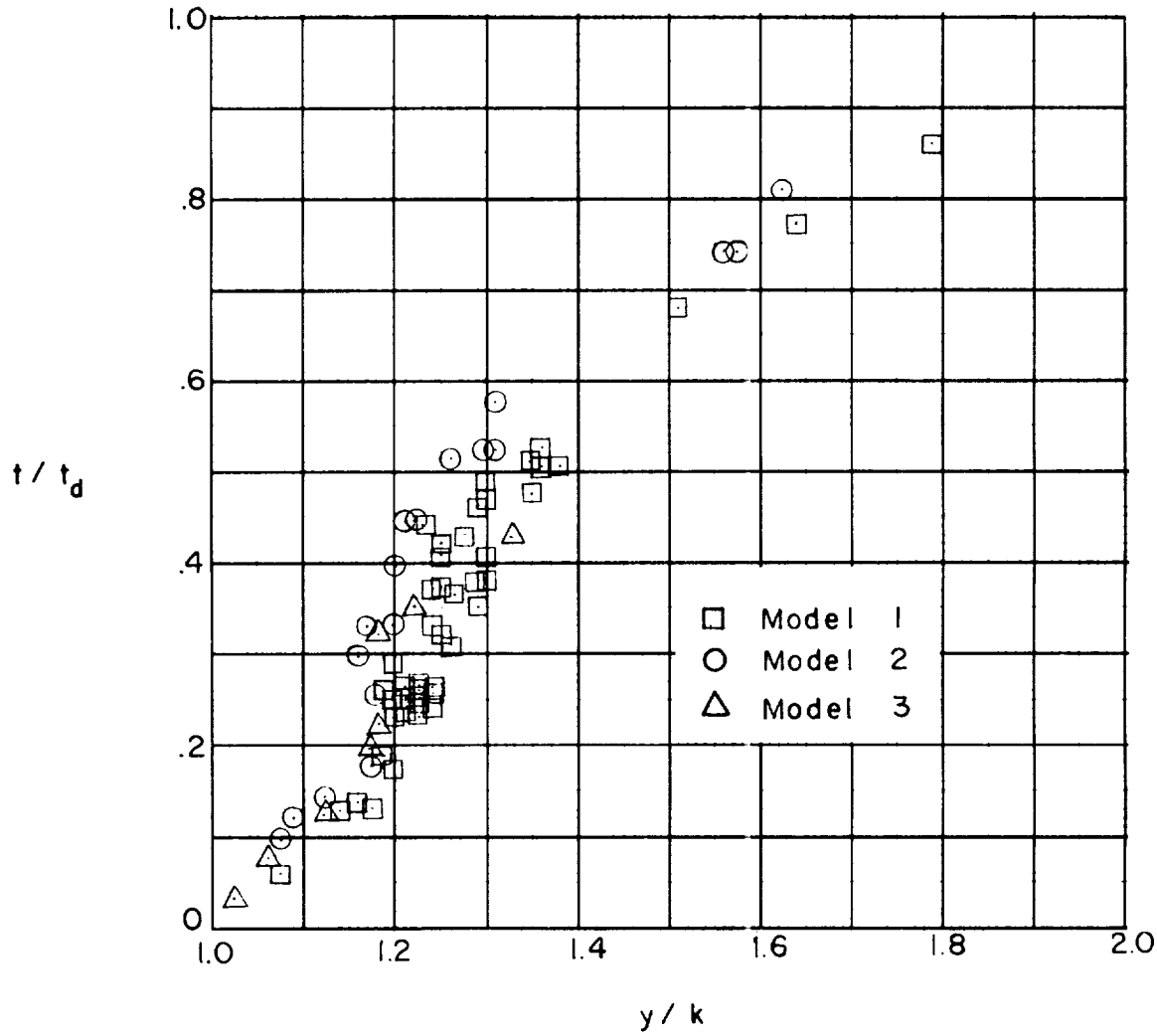

Figure 14.- Vertical component of leading-edge vortex movement with time.

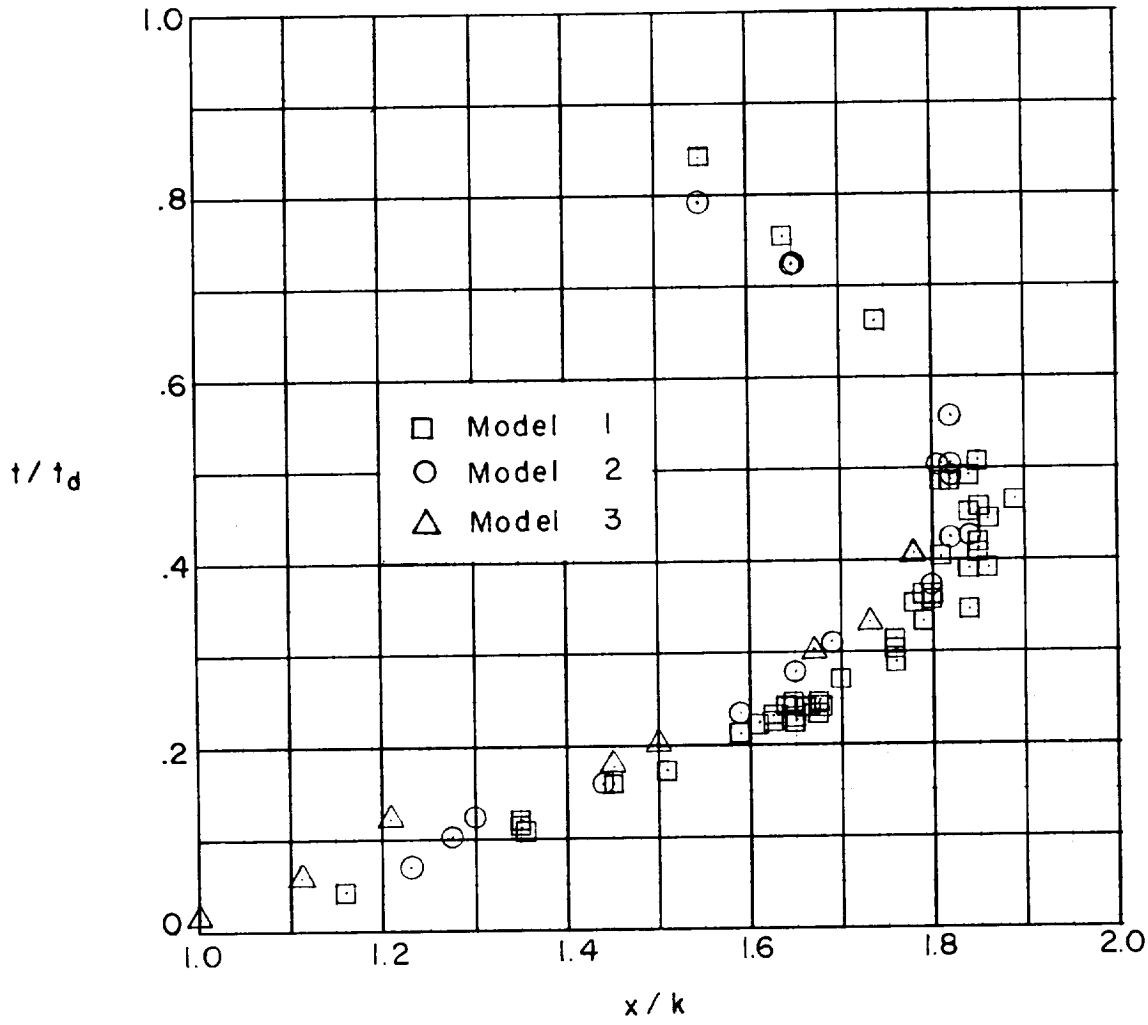

Figure 15.- Horizontal component of trailing-edge vortex movement with time.

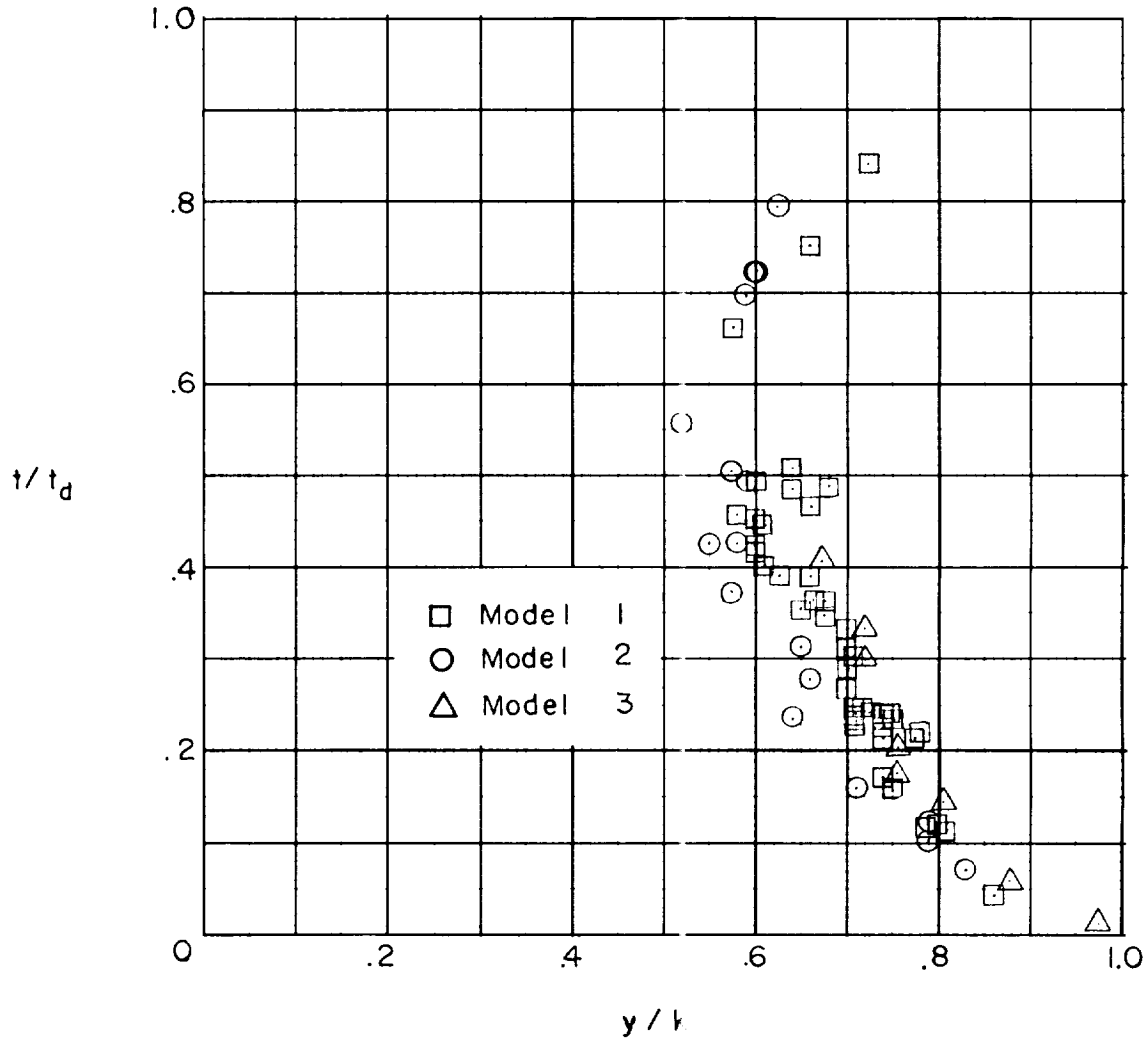

Figure 16.- Vertical component of trailing-edge vortex movement with time.

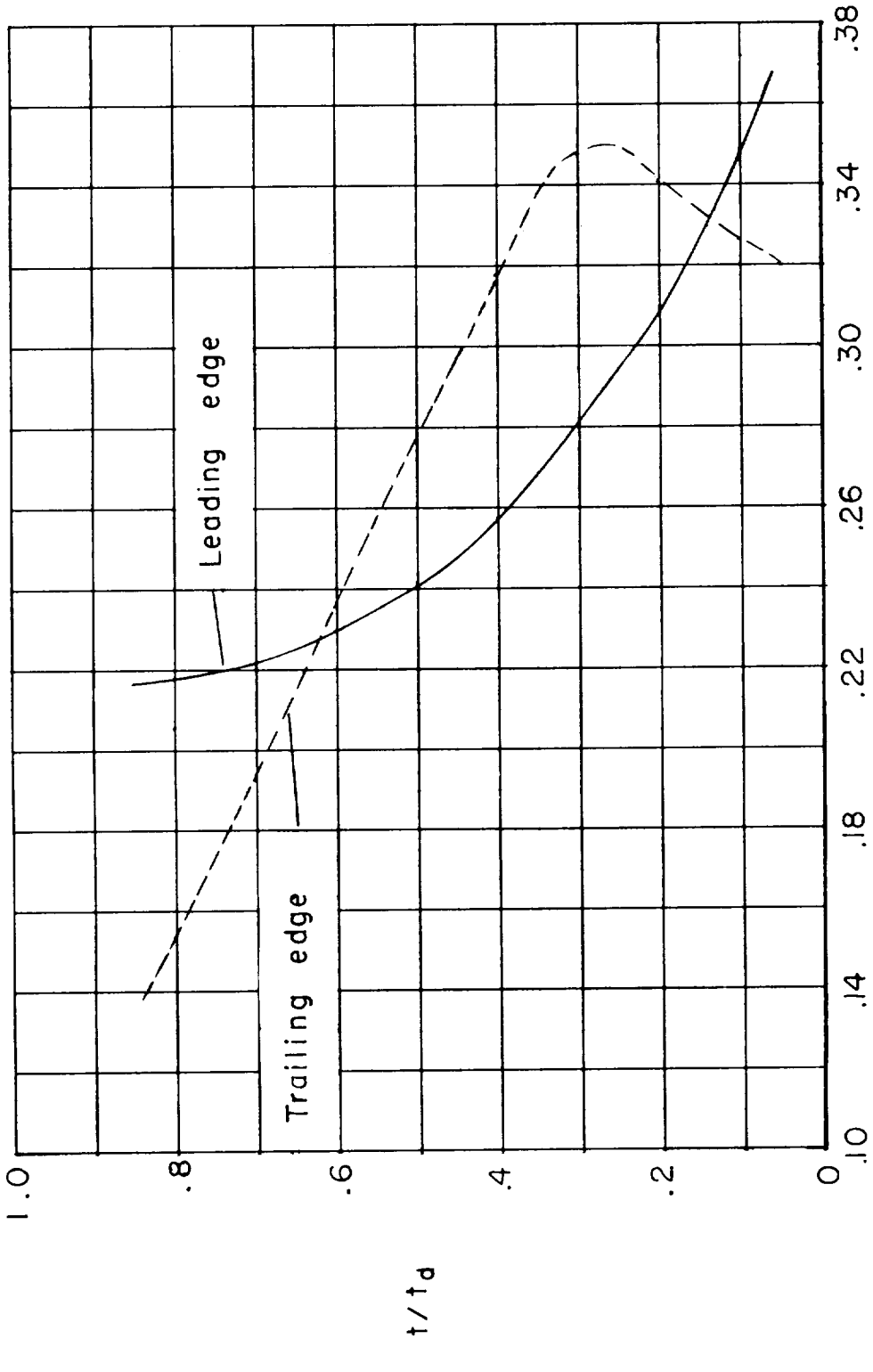

Figure 17.- A comparison of the horizontal components of leading- and trailing-edge vortex movement with respect to free-stream particle movement.

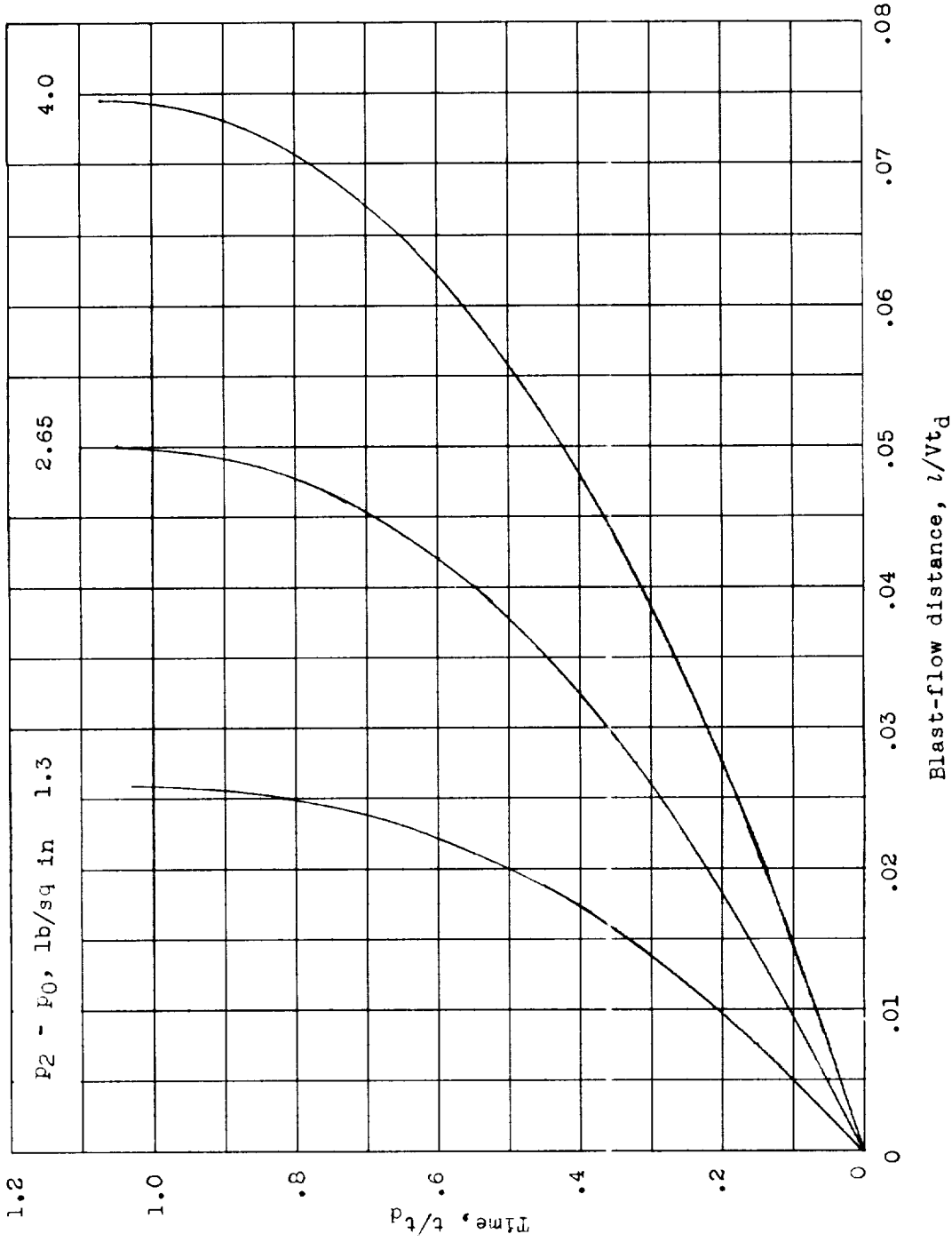

Figure 18.- Nondimensional variation of blast-flow distance with time.